

Uniform spin susceptibility tensor and quasiparticle density of states in organic quasi-one-dimensional superconductors

R. D. Duncan, R. W. Cherng[†], and C. A. R. Sá de Melo
School of Physics, Georgia Institute of Technology, Atlanta Georgia 30332

(Dated: November 21, 2018)

We perform calculations relating the order parameter symmetry of organic quasi-one-dimensional superconductors to the bulk quasiparticle density of states and the bulk uniform spin susceptibility tensor at finite temperatures. Current experimental results suggest that some organic quasi-one-dimensional superconductors may exhibit triplet pairing symmetry. The purpose of our analysis is to attempt to narrow down the number of possibilities for the symmetry of the order parameter based on the current experimental evidence.

PACS numbers: 74.70.Kn

I. INTRODUCTION

After the discovery of quasi-one-dimensional organic superconductors¹, many interesting aspects were studied^{2,3}. The magnetic field versus temperature phase diagram for (TMTSF)₂PF₆ under pressure of 6 kbar was recently revisited by Lee *et al.*⁴. They found that the upper critical fields along the usual **a**, **b'**, and **c*** directions were highly anisotropic. The upper critical field along **a** and **b'** displayed a strong positive curvature at lower temperatures. Furthermore, the slope $[-dH_{c2}/dT]_{T_c}$ for **H** \parallel **b'** was smaller than along the **a** direction, i.e., $H_{c2}^{(a)} > H_{c2}^{(b)}$ at high temperature. While, at low temperatures $H_{c2}^{(b)}$ exceeded $H_{c2}^{(a)}$, after an unusual anisotropy inversion at $H^* = 1.6T$. These initial results suggested the existence of triplet superconductivity in this system. An additional boost for the triplet scenario in (TMTSF)₂PF₆ was given by very recent NMR experiments^{5,6}. Lee *et al.*^{5,6} found that there is **no** ⁷⁷Se Knight shift in (TMTSF)₂PF₆ for fields **H** \parallel **b'** ($P \approx 6$ kbar)⁵, and **H** \parallel **a** ($P \approx 7$ kbar)⁶. These results suggest that $\chi_{b'} \approx \chi_N$, and $\chi_a \approx \chi_N$, where χ_N is the normal state susceptibility. Furthermore, a sharp and narrow (possibly Hebel-Slichter⁷) peak was observed just below T_c in the ⁷⁷Se NMR relaxation rate $1/T_1$, for **H** \parallel **a** ($H = 1.43$ T), and $P \approx 7$ kbar⁶. The combined work of Lee *et al.*^{4,5,6} suggests the existence of a triplet superconducting phase in (TMTSF)₂PF₆. However, these recent ⁷⁷Se NMR results in (TMTSF)₂PF₆ should be contrasted with earlier proton NMR results in (TMTSF)₂ClO₄⁸ which indicated the absence of the coherence peak just below $T_c = 1.03$ K at $H = 0$, and a T^3 behavior between $T_c/2$ and T_c . Based on their experiments, Takigawa *et al.*⁸ argued that the superconducting state of (TMTSF)₂ClO₄ has an anisotropic order parameter vanishing along lines on the Fermi surface, although they were not able to distinguish between singlet and triplet states.

The temperature versus magnetic field phase diagram of (TMTSF)₂ClO₄ at ambient pressure was also measured by Lee *et al.*^{9,10}, for **H** \parallel **b'**. Their results showed that the Pauli paramagnetic limit is also exceeded in this compound. Furthermore, Belin and Behnia¹¹ (BB)

reported measurements of the thermal conductivity in the superconducting state of (TMTSF)₂ClO₄, indicating that their data is inconsistent with the existence of gap nodes at the Fermi surface as suggested by Takigawa *et al.*⁸. BB's argument was that the T^3 behavior of the proton $1/T_1$ ⁸ was limited only to $T > T_c/2$. Thus, it could not be considered convincing evidence for nodes in the gap because the temperature was not low enough. Even for conventionally gapped superconductors, the exponential behavior of $1/T_1$ occurs only at very low temperatures ($T \ll T_c$). Therefore, these recent experimental results combined^{9,10,11} seem to suggest the existence of a fully gapped triplet superconducting state in (TMTSF)₂ClO₄. However, detailed ⁷⁷Se NMR experiments seem to be lacking for (TMTSF)₂ClO₄.

Since both of these materials belong to the same class of compounds and have very similar crystal structures, it is feasible that they may exhibit similar order parameter symmetries. However, additional experiments are necessary in order to make sure that the order parameter symmetry of the (TMTSF)₂ClO₄ is the same as in (TMTSF)₂PF₆. A minimal set of experiments are necessary to identify the symmetry of the order parameter. For instance, data from upper critical field **H** \parallel **a**, ⁷⁷Se Knight shift and NMR relaxation experiments are needed for ClO₄, and information about the thermal conductivity is needed for PF₆. At zero magnetic field, however, these two materials have very different phase diagrams. The compound (TMTSF)₂ClO₄ is superconducting at low temperatures and zero pressure when slowly cooled (R-state), while (TMTSF)₂PF₆ is a spin density wave (SDW) insulator at low temperatures and low pressures, and becomes superconducting at low temperatures only at pressures above 5.5 kbar. Although the similar crystal structure of these systems suggests, from a simple group theoretical point of view, that the origin of the pair interaction is the same, the role of the proximity to an SDW phase in (TMTSF)₂PF₆ needs to be investigated both theoretically and experimentally. Furthermore, the true nature of the order parameter symmetry can only be directly evidenced via phase sensitive experiments like those performed in the cuprate oxides^{12,13}.

Abrikosov was the first to suggest the possibility of

triplet superconductivity in Bechgaard salts^{14,15} based on the behavior of $(\text{TMTSF})_2\text{ClO}_4$ and $(\text{TMTSF})_2\text{PF}_6$ under X-ray bombardment. These systems exhibited a strong suppression of their critical temperature in the presence of radiation induced non-magnetic defects^{16,17}. Gorkov and Jerome¹⁸ also suggested the possibility of triplet superconductivity based on a theoretical extrapolation of the semiclassical upper critical fields calculated near the zero field critical temperature. In addition, Lebed¹⁹ pointed out that triplet superconductivity would manifest itself in Bechgaard salts through a remarkable reentrant phase in high magnetic fields. Later, Dupuis, Montambaux and Sá de Melo (DMS)²⁰ studied the field-versus-temperature phase diagram and the vortex lattice structure of these systems and concluded that these systems could be either in an inhomogeneous singlet state like the Larkin-Ovchinnikov-Fulde-Ferrel (LOFF) state^{21,22} or in a triplet state. Further studies of the LOFF state were performed by Dupuis²³, while an equal spin triplet pairing state (ESTP) was discussed further by Sá de Melo²⁴.

After the upper critical field measurements of Lee *et al.*⁴, Lebed²⁵ was able to show that the LOFF state was Pauli paramagnetically limited, thus giving further support for the triplet scenario (at least at high magnetic fields). The possibility of a magnetic field induced singlet (low fields) to triplet (high fields) transition was considered by Sá de Melo^{26,27} and Vaccarella and Sá de Melo²⁸, but currently there is no experimental evidence of a kink in the upper critical field of these systems. Furthermore, reentrant superconductivity was still expected for the triplet state at high magnetic fields^{25,28}. All these previous theories neglected the effects of fluctuations at high magnetic fields. A first attempt to incorporate fluctuation effects was made recently by Vaccarella and Sá de Melo²⁹ who showed that phase fluctuations can suppress the reentrant phase at high magnetic fields in the ESTP state. Very recently Lebed, Machida and Ozaki (LMO)³⁰ suggested the possibility of a triplet phase with a \mathbf{d} -vector with zero-component along the \mathbf{b}' axis and a finite component along the \mathbf{a} axis. A direct consequence of LMO's proposal is the existence of an anisotropic spin susceptibility at zero temperature and low magnetic fields: $\chi_{b'} = \chi_N$, and $\chi_a \ll \chi_N$, where χ_a corresponds to $\mathbf{H} \parallel \mathbf{a}$, $\chi_{b'}$ corresponds to $\mathbf{H} \parallel \mathbf{b}'$, and χ_N corresponds to the normal state susceptibility. However, Lee *et al.*^{5,6} reported new ⁷⁷Se NMR (Knight shift) results for $(\text{TMTSF})_2\text{PF}_6$ under pressure, indicating that $\chi_{b'} \approx \chi_N$, and $\chi_a \approx \chi_N$. A fully gapped singlet “d-wave” order parameter for $(\text{TMTSF})_2\text{ClO}_4$ was proposed by Shimahara³¹, while gapless triplet “f-wave” superconductivity for $(\text{TMTSF})_2\text{PF}_6$ was proposed by Kuroki, Arita, and Aoki (KAA)³². Duncan, Vaccarella, and Sá de Melo (DVS)³³ performed a group theoretical analysis and suggested that a weak spin-orbit fully gapped triplet “ p_x -wave” order parameter would be a good candidate for superconductivity in Bechgaard salts. For this symmetry $\chi_a \approx \chi_N$, and $\chi_{b'} \approx \chi_N$ ^{26,27,33} in agreement with experimental results^{5,6}. In addition, this order parameter

choice is consistent with the expectation of weak atomic spin-orbit effects, given that the heaviest element in these systems is Se.

This paper is a longer version of the brief report by DVS³³. Here, we are concerned mostly with the symmetry of the order parameter of a triplet quasi-one-dimensional superconductor at zero magnetic field, and have three main goals. First, we perform a group theoretical analysis of the possible symmetries of the order parameter for an orthorhombic quasi-one-dimensional superconductor. Second, we calculate the temperature dependence of the bulk quasiparticle density of states and of the bulk uniform spin susceptibility tensor for various candidate symmetries of the order parameter consistent with the group theoretical analysis. Third, we make connections to scanning tunneling microscopy (STM) of quasiparticle density of states and Knight shift measurements of the spin susceptibility tensor. Thus, the remainder of the paper is organized as follows. In section II, we discuss the Hamiltonian used for weak spin-orbit (strong spin-orbit) coupling cases for generic singlet (pseudo-singlet) and triplet (pseudo-triplet) states. In section III, we perform a group theoretical analysis of the symmetry of the order parameter, both in the weak and strong spin-orbit coupling limits. In section IV, we discuss the quasiparticle density of states for different symmetries of the order parameter. In addition, in section V, we analyse the uniform spin susceptibility tensor χ_{mn} for several order parameter symmetries, and we discuss finite magnetic field effects and the role of vortices on χ_{mn} . Finally, we summarize our results in section VI.

II. HAMILTONIAN

In order to analyze the possible different symmetries of the order parameter we study quasi-one-dimensional systems with a single band in an orthorhombic lattice and allow for singlet or triplet pairing. We consider the following dispersion relation

$$\epsilon_{\mathbf{k}} = -|t_x| \cos(k_x a) - |t_y| \cos(k_y b) - |t_z| \cos(k_z c), \quad (1)$$

where $|t_x| \gg |t_y| \gg |t_z|$. Note that this notation is slightly different from the standard notation². The corresponding translation is $|t_x| \rightarrow 2t_a$; $|t_y| \rightarrow 2t_b$; $|t_z| \rightarrow 2t_c$. Furthermore, a , b and c in our notation correspond to the unit cell lengths along the crystallographic directions \mathbf{a} , \mathbf{b}' , and \mathbf{c}^* respectively. In the limit of weak interactions and low densities these quasi-one-dimensional systems exhibit a well defined Fermi surface which is open, being formed of two separate sheets which intersect the Brillouin zone boundaries in the k_y and k_z directions. We work with the Hamiltonian

$$H = H_{kin} + H_{int}, \quad (2)$$

where the kinetic energy part is

$$H_{kin} = \sum_{\mathbf{k}, \alpha} (\epsilon_{\mathbf{k}} - \mu) \psi_{\mathbf{k}, \alpha}^\dagger \psi_{\mathbf{k}, \alpha}, \quad (3)$$

where $\epsilon_{\mathbf{k}}$ is the dispersion defined in Eq. 1, μ is the chemical potential, and

$$H_{int} = \frac{1}{2} \sum_{\mathbf{k} \mathbf{k}' \mathbf{q}} \sum_{\alpha \beta \gamma \delta} V_{\alpha \beta \gamma \delta}(\mathbf{k}, \mathbf{k}') b_{\alpha \beta}^\dagger(\mathbf{k}, \mathbf{q}) b_{\gamma \delta}(\mathbf{k}', \mathbf{q}) \quad (4)$$

is the interaction part with

$$b_{\alpha \beta}^\dagger(\mathbf{k}, \mathbf{q}) = \psi_{-\mathbf{k} + \mathbf{q}/2, \alpha}^\dagger \psi_{\mathbf{k} + \mathbf{q}/2, \beta}^\dagger, \quad (5)$$

where the labels α, β, γ and δ are spin indices and the labels \mathbf{k}, \mathbf{k}' and \mathbf{q} represent linear momenta.

In the case of weak spin-orbit coupling and triplet pairing ($S = 1$), the model interaction tensor can be chosen to be

$$V_{\alpha \beta \gamma \delta}(\mathbf{k}, \mathbf{k}') = \Gamma_{\alpha \beta \gamma \delta} V_\Gamma(\mathbf{k}, \mathbf{k}') \phi_\Gamma(\mathbf{k}) \phi_\Gamma^*(\mathbf{k}'), \quad (6)$$

where $\Gamma_{\alpha \beta \gamma \delta} = \mathbf{v}_{\alpha \beta} \cdot \mathbf{v}_{\gamma \delta}^\dagger / 2$ with $\mathbf{v}_{\alpha \beta} = (i\sigma\sigma_y)_{\alpha \beta}$. In addition, the interaction V_Γ corresponds to the irreducible representation Γ with basis function $\phi_\Gamma(\mathbf{k})$ representative of the orthorhombic group. In the case of strong spin-orbit coupling and $S = 1$ the interaction

$$V_{\alpha \beta \gamma \delta}(\mathbf{k}, \mathbf{k}') = V_\Gamma(\mathbf{k}, \mathbf{k}') [\Phi_\Gamma(\mathbf{k}) \cdot \mathbf{v}_{\alpha \beta}] [\Phi_\Gamma^*(\mathbf{k}') \cdot \mathbf{v}_{\gamma \delta}^\dagger] / 2 \quad (7)$$

where the interaction V_Γ corresponds to the irreducible representation Γ with basis function vector $\Phi_\Gamma(\mathbf{k})$ representative of the orthorhombic group. In both weak and strong spin-orbit coupling, we use either the equation of motion method³⁴ or the functional integration method^{35,36} in the zero center of mass momentum pairing approximation (which corresponds to the BCS limit in weak coupling) to obtain the anomalous Green's function

$$F_{\alpha \beta}(\mathbf{k}, i\omega_n) = \frac{\Delta_{\alpha \beta}(\mathbf{k})}{\omega_n^2 + E_{\mathbf{k}}^2}, \quad (8)$$

and the single particle Green's function

$$G_{\alpha \beta}(\mathbf{k}, i\omega_n) = -\frac{i\omega_n + \xi_{\mathbf{k}}}{\omega_n^2 + E_{\mathbf{k}}^2} \delta_{\alpha \beta}, \quad (9)$$

where $\xi_{\mathbf{k}} = \epsilon_{\mathbf{k}} - \mu$ is the dispersion $\epsilon_{\mathbf{k}}$ relative to the chemical potential μ ,

$$E_{\mathbf{k}} = \sqrt{\xi_{\mathbf{k}}^2 + \Delta_{\mathbf{k}}^2} \quad (10)$$

is the quasiparticle excitation energy, and

$$\Delta_{\mathbf{k}}^2 \equiv \text{Tr} [\tilde{\Delta}^\dagger(\mathbf{k}) \tilde{\Delta}(\mathbf{k})] / 2, \quad (11)$$

where the order parameter matrix $\tilde{\Delta}(\mathbf{k})$ has elements $\Delta_{\alpha \beta}(\mathbf{k})$. The expressions for the anomalous (Eq. 8) and for the single particle (Eq. 9) Green's functions are valid only in the unitary case where $\tilde{\Delta}^\dagger(\mathbf{k}) \tilde{\Delta}(\mathbf{k})$ is diagonal. In this initial work, we do not discuss in detail the non-unitary case for triplet superconductivity. Using the single particle and anomalous Green's functions defined above and standard many body methods^{34,35,36}, we derive the order parameter equation in terms of the anomalous Green's function as

$$\Delta_{\alpha \beta}(\mathbf{k}) = -T \sum_{\omega_n, \mathbf{k}'} V_{\beta \alpha \gamma \delta}(\mathbf{k}, \mathbf{k}') F_{\gamma \delta}(\mathbf{k}'), \quad (12)$$

while the number equation, that fixes the chemical potential μ , can be written as

$$N = -T \sum_{\omega_n, \mathbf{k}} \text{Tr} \left[\tilde{G}(\mathbf{k}, i\omega_n) \frac{\partial}{\partial \mu} \tilde{G}^{-1}(\mathbf{k}, i\omega_n) \right]. \quad (13)$$

The matrix $\tilde{G}(\mathbf{k}, i\omega_n)$ is the 2×2 block matrix

$$\tilde{G}(\mathbf{k}, i\omega_n) = \begin{pmatrix} G_{\alpha \beta}(\mathbf{k}, i\omega_n) & -F_{\alpha \beta}(\mathbf{k}, i\omega_n) \\ -F_{\alpha \beta}^\dagger(\mathbf{k}, i\omega_n) & -G_{\beta \alpha}(-\mathbf{k}, -i\omega_n) \end{pmatrix}, \quad (14)$$

with matrix elements which are in turn 2×2 matrices in spin space. Performing the Matsubara sums and traces in Eq. (12) and Eq. (13) we obtain the more familiar forms

$$\Delta_{\alpha \beta}(\mathbf{k}) = - \sum_{\mathbf{k}'} V_{\beta \alpha \gamma \delta}(\mathbf{k}, \mathbf{k}') \frac{\Delta_{\gamma \delta}(\mathbf{k}')}{2E_{\mathbf{k}'}} \tanh \left(\frac{E_{\mathbf{k}'}}{2T} \right), \quad (15)$$

$$N \equiv \sum_{\mathbf{k}} n_{\mathbf{k}} = \sum_{\mathbf{k}} \left[\left(1 + \frac{\xi_{\mathbf{k}}}{E_{\mathbf{k}}} \right) f(E_{\mathbf{k}}) + \left(1 - \frac{\xi_{\mathbf{k}}}{E_{\mathbf{k}}} \right) (1 - f(E_{\mathbf{k}})) \right], \quad (16)$$

for the order parameter and number equations, re-

spectively. These two equations must be solved self-

consistently away from the strict BCS limit in order to accommodate particle-hole asymmetries and strong coupling effects which tend to shift the chemical potential substantially away from the Fermi energy. Quite generally these two equations are correct even in the strong coupling (or low density) regime provided that $T \ll T_c^{35,36}$.

III. POSSIBLE SYMMETRIES FOR THE ORDER PARAMETER

We will now discuss the symmetry of the order parameter $\Delta_{\alpha\beta}$. For this purpose, we consider an orthorhombic crystal³⁷ with a conventional symmetry normal state, i.e., we assume that the normal state does not break the full lattice symmetry. By contrast, normal states that break full lattice symmetry are spatially inhomogeneous. Examples of such spatially inhomogeneous states are stripe phases that occur in high- T_c superconductors, magnetic normal phases (ferro and antiferromagnetic), and normal states in a magnetic field (where the magnetic translation group needs to be incorporated). These states, however, will not be considered in the analysis performed in this section.

In the case of weak spin-orbit coupling, the most general conventional symmetry group for the normal state is $G_n = \text{SO}(3) \times G_c \times \text{U}(1) \times \text{T}$, where $\text{SO}(3)$ is the group of rotations in spin space, G_c is the crystal space group, $\text{U}(1)$ is the gauge group and T corresponds to time reversal symmetry. Here, rotations of the spin and spatial degrees of freedom are independent. Since the superconducting state breaks $\text{U}(1)$ symmetry, the possible order parameters correspond to different irreducible representations of $G_s = \text{SO}(3) \times G_c$. However, in the case of strong spin-orbit coupling the normal state symmetry group is $G_n = G_c^{(J)} \times \text{U}(1) \times \text{T}$, where now $G_c^{(J)}$ is identical to the space group G_c except when a rotation is involved. In this case, rotations of the spin and spatial degrees of freedom are not independent, and the possible order parameters correspond to different irreducible representations of $G_s = G_c^{(J)}$. Although spin is not a good quantum number when spin-orbit coupling is important, we will still classify the possible states as singlet or triplet with respect to a pseudo-spin space provided that the superconducting state does not break inversion symmetry. The singlet/triplet pseudo-spin classification was first introduced by Anderson³⁸ in the context of heavy fermions. We will use this classification here whenever we refer to strong spin-orbit representations. Considering quasi-one-dimensional superconductors of orthorhombic crystal structure³⁷, the relevant crystallographic point group is D_{2h} , which has only one dimensional representations³⁹ (See Table I).

A. General Order Parameter

The general form of the order parameter is

$$\tilde{\Delta}(\mathbf{k}) = i (\Delta_{si}(\mathbf{k})\tilde{\mathbf{1}} + \Delta_{tr}(\mathbf{k})\mathbf{d}(\mathbf{k}) \cdot \boldsymbol{\sigma}) \sigma_y, \quad (17)$$

which must transform according to the one dimensional representations of the orthorhombic point group D_{2h} , under the assumption that the order parameter does not break the crystal translational symmetry, i.e., the order parameter is invariant under all primitive lattice translations. The matrix $\tilde{\mathbf{1}}$ is the identity and the function $\Delta_{si}(\mathbf{k})$ is symmetric (even) under the transformation $\mathbf{k} \rightarrow -\mathbf{k}$. The three-dimensional vector $\mathbf{d}(\mathbf{k})$ is antisymmetric (odd) under $\mathbf{k} \rightarrow -\mathbf{k}$, while the function $\Delta_{tr}(\mathbf{k})$ is symmetric (even) under the transformation $\mathbf{k} \rightarrow -\mathbf{k}$.

We are mostly interested in triplet states which do not break time reversal symmetry, and our analysis is confined initially to zero magnetic field. However, for completeness, we shall mention briefly singlet and time-reversal-symmetry-breaking triplet states. In Table II, a summary of the possible order parameter symmetries consistent with the D_{2h} point group is presented for singlet systems assuming weak spin-orbit coupling, while in Table III a summary of the possible order parameter symmetries for time-reversal-symmetry-breaking triplet states is shown. Tables IV and V summarize the group theoretical analysis performed for the order parameter matrix $\tilde{\Delta}(\mathbf{k})$ for time-reversal-invariant triplet superconductors in the weak and strong spin-orbit coupling cases, respectively. All the tables mentioned above include the state nomenclature, the order parameter for the respective singlet or triplet symmetries, and the loci of zeros of the corresponding quasiparticle excitation spectrum $E_{\mathbf{k}}$, when $\tilde{\mu} = \mu - \min[\epsilon_{\mathbf{k}}]$ is positive. In Table IV, the vector (0,0,1) is indicated up to an arbitrary rotation in spin space. In Table V, the numerical coefficients A, B and C define a specific model for the strong spin-orbit interaction appearing in Eq. (7). It is very important to emphasize here that the basis functions $X(\mathbf{k})$, $Y(\mathbf{k})$ and $Z(\mathbf{k})$ transform like k_x , k_y and k_z , respectively, under the crystallographic point group operations, but they can not be chosen to be equal to k_x , k_y and k_z . The reason being that the normal state dispersion $\epsilon_{\mathbf{k}}$ intersects the boundary of the Brillouin zone along the k_y and k_z directions. Thus, it is necessary to take into account the periodicity of the order parameter matrix $\tilde{\Delta}(\mathbf{k})$ and of the order parameter vector $\mathbf{d}(\mathbf{k})$ in reciprocal (momentum) space. In the case of orthorhombic crystals with dispersion $\epsilon_{\mathbf{k}}$ defined in Eq. (1), where $|t_x| \gg |t_y| \gg |t_z|$ a Fermi surface exists (for weak attractive interaction or high densities) and does intersect the Brillouin zones, therefore the minimal basis set must be periodic and may be chosen to be $X(\mathbf{k}) = \sin(k_x a)$, $Y(\mathbf{k}) = \sin(k_y b)$ and $Z(\mathbf{k}) = \sin(k_z c)$.

TABLE I: Character table for the D_{2h} point group.

| Representation | E | C_2^z | C_2^y | C_2^x | i | iC_2^z | iC_2^y | iC_2^x | Basis |
|----------------|-----|---------|---------|---------|-----|----------|----------|----------|-------|
| A_{1g} | 1 | 1 | 1 | 1 | 1 | 1 | 1 | 1 | 1 |
| B_{1g} | 1 | 1 | -1 | -1 | 1 | 1 | -1 | -1 | XY |
| B_{2g} | 1 | -1 | 1 | -1 | 1 | -1 | 1 | -1 | XZ |
| B_{3g} | 1 | -1 | -1 | 1 | 1 | -1 | -1 | 1 | YZ |
| A_{1u} | 1 | 1 | 1 | 1 | -1 | -1 | -1 | -1 | XYZ |
| B_{1u} | 1 | 1 | -1 | -1 | -1 | -1 | 1 | 1 | Z |
| B_{2u} | 1 | -1 | 1 | -1 | -1 | 1 | -1 | 1 | Y |
| B_{3u} | 1 | -1 | -1 | 1 | -1 | 1 | 1 | -1 | X |

TABLE II: Time reversal invariant singlet states in an orthorhombic crystal, assuming weak spin-orbit coupling.

| State | Residual Group | Order parameter $\Delta_{si}(\mathbf{k})$ | $E_{\mathbf{k}} = 0$ ($\tilde{\mu} > 0$) | $E_{\mathbf{k}} = 0$ ($\tilde{\mu} < 0$) |
|------------|--|---|--|--|
| $^1A_{1g}$ | $SO_3 \times D_{2h} \times T$ | 1 | none | none |
| $^1B_{1g}$ | $SO_3 \times D_2(C_2^z) \times I \times T$ | XY | lines | none |
| $^1B_{2g}$ | $SO_3 \times D_2(C_2^y) \times I \times T$ | XZ | lines | none |
| $^1B_{3g}$ | $SO_3 \times D_2(C_2^x) \times I \times T$ | YZ | lines | none |

B. Excitation Spectrum Characteristics

For the weak spin-orbit coupling (Table IV) the only candidate for weaker attractive interaction ($\tilde{\mu} > 0$) is the state $^3B_{3u}(a)$, where the quasiparticle excitation spectrum $E_{\mathbf{k}}$ is fully gapped. In the case of strong spin-orbit coupling (Table V) there are three candidates for weaker attractive interaction ($\tilde{\mu} > 0$), i.e., the states A_{1u} , B_{1u} and B_{2u} , where the quasiparticle excitation spectrum $E_{\mathbf{k}}$ may be fully gapped. When $\tilde{\mu} > 0$, the state A_{1u} is fully gapped only for $A \neq 0$ and for any value of B and C ; the state B_{1u} is fully gapped only for $B \neq 0$ and for any value of A and C ; and the state B_{2u} is fully gapped only for $C \neq 0$ and for any value of A and B .

We note in passing that in the case of strong attractive interactions or small densities, where $\tilde{\mu} < 0$, the excitation spectrum $E_{\mathbf{k}}$ is fully gapped⁴⁰ for all of the states involving Tables IV and V, for example. Therefore, if Field Effect Transistor (FET) systems^{41,42} can be constructed to change the density of carriers (n) in quasi-one-dimensional organic superconductors, it may be possible to study systematically the carrier density dependence of physical properties in these systems. The most interesting theoretical case corresponds to the situation where $E_{\mathbf{k}}$ has zeros for $\tilde{\mu} > 0$ ($n > n_c$), and $E_{\mathbf{k}}$ has a full gap for $\tilde{\mu} < 0$ ($n < n_c$). Here n_c is the critical density where $\tilde{\mu} = 0$, where the characteristics of excitation energy $E_{\mathbf{k}}$ changes in a fundamental way. This effect here should correspond to a Lifshitz transition for superconductors⁴⁰ where low temperature properties like spin susceptibility, specific heat, thermal conductivity, would change their qualitative behavior depending on n being greater, equal or less than n_c . The Lifshitz transition should also be accompanied by a topological phase tran-

sition in the ground state⁴⁰, where the zero temperature electronic compressibility diverges at $n = n_c$. However, if the excitation spectrum $E_{\mathbf{k}}$ is fully gapped (like in the case of the $^3B_{3u}(a)$ state) for $\tilde{\mu} > 0$ ($n > n_c$), $E_{\mathbf{k}}$ would remain fully gapped for $\tilde{\mu} < 0$ ($n < n_c$), and only a crossover should occur.

We also note in passing, that the states shown in Table III are non-unitary since they break time reversal symmetry. In this case the excitation spectrum has two branches and is given by

$$E_{\mathbf{k}\pm} = \sqrt{\xi_k^2 + |\Delta_{tr}(\mathbf{k})|^2 [|\mathbf{d}(\mathbf{k})|^2 \pm |\mathbf{q}(\mathbf{k})|]},$$

where $\mathbf{q}(\mathbf{k}) = i\mathbf{d}^*(\mathbf{k}) \times \mathbf{d}(\mathbf{k})$. For $\tilde{\mu} > 0$ ($n > n_c$), the regions in momentum space where $E_{\mathbf{k}-} = 0$ correspond to surfaces, while the regions where $E_{\mathbf{k}+} = 0$ correspond to lines or the null set, as indicated in Table III. Thus, for $\tilde{\mu} > 0$ ($n > n_c$), the excitation spectrum is gapless. However, for $\tilde{\mu} < 0$ ($n < n_c$), there are no regions in momentum space where $E_{\mathbf{k}\pm} = 0$, which means that the superconductor becomes fully gapped. This dramatic change in the excitation spectrum (from gapless to fully gapped) of time reversal breaking (non-unitary) triplet states should also correspond to a Lifshitz transition at finite temperatures and a topological transition in the ground state⁴⁰. Although, there is currently no experimental evidence that quasi-one-dimensional superconductor break time reversal symmetry (at zero magnetic field), it seems that in the case of Strontium Ruthenate time reversal symmetry breaking states are potentially good candidates for the order parameter⁴³. Strontium Ruthenate is very different from Bechgaard salts since it is non-organic and has essentially a tetragonal quasi-two-dimensional structure. If Field Effect Transistor (FET)

TABLE III: Time reversal breaking triplet states in an orthorhombic crystal, assuming weak spin-orbit coupling.

| State | Residual Group | Order parameter $\mathbf{d}(\mathbf{k})$ | $E_{\mathbf{k}\pm} = 0$ ($\tilde{\mu} > 0$) | $E_{\mathbf{k}\pm} = 0$ ($\tilde{\mu} < 0$) |
|---------------|---|--|---|---|
| $^3A_{1u}(b)$ | $D_{\infty}(E) \times D_2 \times I(E)$ | $(1, i, 0)XYZ$ | surface (-), lines (+) | none |
| $^3B_{1u}(b)$ | $D_{\infty}(E) \times D_2(C_2^z) \times I(E)$ | $(1, i, 0)Z$ | surface (-), lines (+) | none |
| $^3B_{2u}(b)$ | $D_{\infty}(E) \times D_2(C_2^y) \times I(E)$ | $(1, i, 0)Y$ | surface (-), lines (+) | none |
| $^3B_{3u}(b)$ | $D_{\infty}(E) \times D_2(C_2^x) \times I(E)$ | $(1, i, 0)X$ | surface (-), none (+) | none |

TABLE IV: Time reversal invariant triplet states in an orthorhombic crystal, assuming weak spin-orbit coupling.

| State | Residual Group | Order parameter $\mathbf{d}(\mathbf{k})$ | $E_{\mathbf{k}} = 0$ ($\tilde{\mu} > 0$) | $E_{\mathbf{k}} = 0$ ($\tilde{\mu} < 0$) |
|---------------|---|--|--|--|
| $^3A_{1u}(a)$ | $D_{\infty}(C_{\infty}) \times D_2 \times I(E) \times T$ | $(0, 0, 1)XYZ$ | lines | none |
| $^3B_{1u}(a)$ | $D_{\infty}(C_{\infty}) \times D_2(C_2^z) \times I(E) \times T$ | $(0, 0, 1)Z$ | lines | none |
| $^3B_{2u}(a)$ | $D_{\infty}(C_{\infty}) \times D_2(C_2^y) \times I(E) \times T$ | $(0, 0, 1)Y$ | lines | none |
| $^3B_{3u}(a)$ | $D_{\infty}(C_{\infty}) \times D_2(C_2^x) \times I(E) \times T$ | $(0, 0, 1)X$ | none | none |

TABLE V: Time reversal invariant triplet states in an orthorhombic crystal, assuming strong spin-orbit coupling.

| State | Residual Group | Order parameter $\mathbf{d}(\mathbf{k})$ | $E_{\mathbf{k}} = 0$ ($\tilde{\mu} > 0$) | $E_{\mathbf{k}} = 0$ ($\tilde{\mu} < 0$) |
|----------|-----------------------------------|--|--|--|
| A_{1u} | $D_2 \times I(E) \times T$ | (AX, BY, CZ) | none, points, lines | none |
| B_{1u} | $D_2(C_2^z) \times I(E) \times T$ | $(AY, BX, CXYZ)$ | none, lines | none |
| B_{2u} | $D_2(C_2^y) \times I(E) \times T$ | $(AZ, BXYZ, CX)$ | none, lines | none |
| B_{3u} | $D_2(C_2^x) \times I(E) \times T$ | $(AXYZ, BZ, CY)$ | points, lines | none |

systems^{41,42} can be constructed to change the density of carriers (n) in Strontium Ruthenate, it may be also possible: (a) to study systematically the carrier density dependence of physical properties; (b) to search for a possible Lifshitz transition at finite temperatures, and (c) to investigate a possible topological quantum phase transition in the ground state.

C. Three Dimensional Views of the Order Parameter

A three dimensional view of the Fermi surface and order parameter sign for possible weak spin-orbit coupling singlet states compatible with the orthorhombic (D_{2h}) group are shown in Fig. 1 for the case where $\tilde{\mu} > 0$. In Fig. 1(a), (b), (c) and (d) the signs of the orbital component of the order parameter are shown for the $^1A_{1g}$ (“s-wave”), $^1B_{1g}$ (“ d_{xy} -wave”), $^1B_{2g}$ (“ d_{xz} -wave”), $^1B_{1g}$ (“ d_{yz} -wave”), respectively. The nodes are indicated by the dark thick lines separating the order parameter signs. In Fig. 2 a three dimensional view of the Fermi surface and order parameter sign for possible weak-spin orbit coupling triplet states compatible with the orthorhombic (D_{2h}) group are shown for the case where $\tilde{\mu} > 0$. In Fig. 2(a), (b), (c) and (d) the signs of the orbital component of the order parameter are shown for the $^3A_{1u}(a)$ (“ f_{xyz} -wave”), $^3B_{1u}(a)$ (“ p_z -wave”), $^3B_{2u}(a)$ (“ p_y -wave”), $^3B_{1u}(a)$ (“ p_x -wave”), re-

spectively.

For the weak spin-orbit states is not only useful to know where the orbital components of the order parameter change sign, but it is also important to visualize the \mathbf{d} -vector at the Fermi surface. In the complete absence of the spin-orbit coupling the \mathbf{d} -vectors can point in any direction with equal probability. However Bechgaard salts are expected to have weak spin-orbit coupling, leading to the weak pinning of the \mathbf{d} -vector along a preferred direction. Based on recent ^{77}Se NMR experiments^{5,6} it seems that the \mathbf{d} -vector in $(\text{TMTSF})_2\text{PF}_6$ is not pointing along \mathbf{a} or \mathbf{b}' direction at least for magnetic fields beyond the 1 T range. Therefore, in Fig. 3 we choose the weak spin-orbit coupling \mathbf{d} -vectors to be pointing along the \mathbf{c} direction. We also illustrate in Fig. 4 the \mathbf{d} -vector structure for the case of strong spin-orbit coupling. The \mathbf{d} -vector for the states A_{1u} , B_{1u} , B_{2u} , and B_{3u} (see Table V are shown in Figs. 4a, 4b, 4c, and 4d, for $A = B = 1$ and $C = 0$, respectively. Notice the textured structure of the \mathbf{d} -vectors at the Fermi surface.

As discussed in the introduction the combined experimental evidence of the upper critical field measurements of Lee *et. al.*^{4,9,10}, thermal conductivity measurements of BB¹¹, and the Knight shift and NMR relaxation experiments of Lee *et. al.*^{5,6}, suggest that $(\text{TMTSF})_2\text{ClO}_4$ and/or $(\text{TMTSF})_2\text{PF}_6$ may be fully gapped triplet superconductors. Thus, we consider next the temperature dependences of the quasiparticle density of states (QDOS) and of the uniform spin susceptibility tensor for a few po-

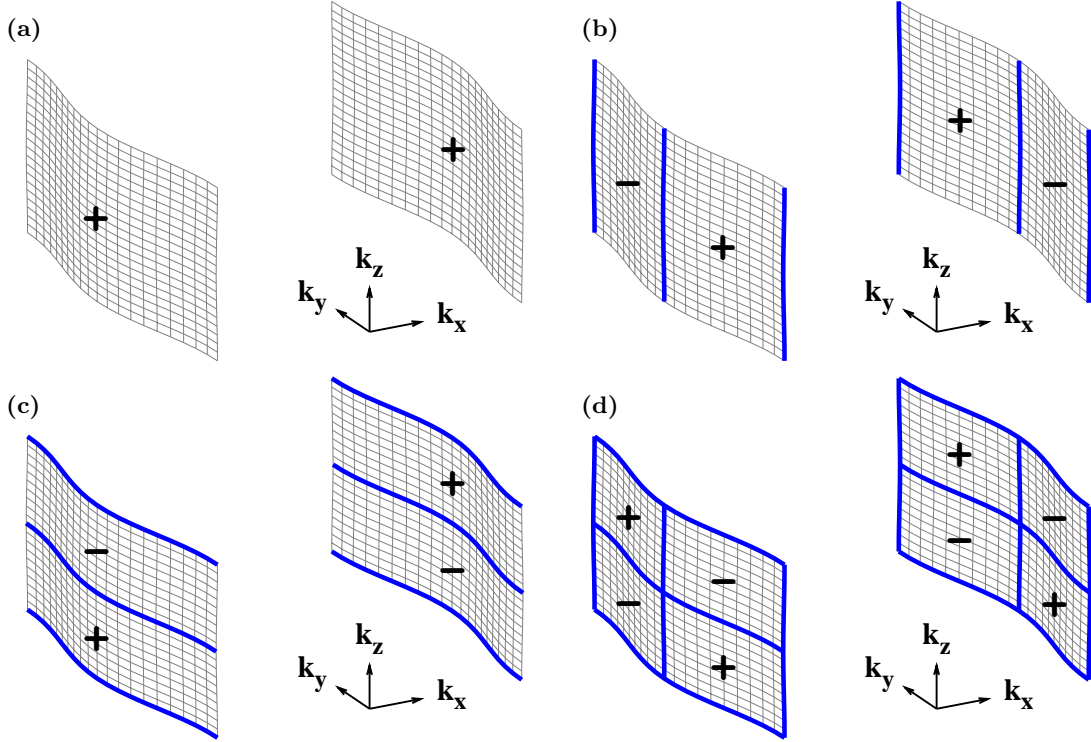


FIG. 1: Three dimensional views of the sign of the orbital component of the order parameter. Various weak spin-orbit coupling order parameter symmetries are illustrated (See Table II): (a) $^1A_{1g}$ (“s-wave”); (b) $^1B_{1g}$ (“ d_{xy} -wave”); (c) $^1B_{2g}$ (“ d_{xz} -wave”); (d) $^1B_{3g}$ (“ d_{yz} -wave”). The thick lines correspond to the zeros of the orbital parts of the order parameter as well as to the excitation energy node structure ($E_{\mathbf{k}} = 0$) on the Fermi surface ($\bar{\mu} > 0$).

tential triplet candidate states, which are fully gapped: a) the weak spin-orbit coupling state $^3B_{3u}(a)$ of Table IV; b) the strong spin-orbit coupling states A_{1u} of table V with $A \neq 0$. Other fully gapped triplet states correspond to the B_{1u} and B_{2u} of table V with $B \neq 0$, and $C \neq 0$, respectively. We will not discuss these states any further here. However, we will make comparisons of the chosen triplet candidates with the results of reference singlet states $^1A_{1g}$ (“s-wave”) and $^1B_{1g}$ (“ d_{xy} -wave”).

IV. QUASIPARTICLE DENSITY OF STATES

The bulk quasiparticle density of states (QDOS) for these different symmetries can be obtained from the single particle Green’s function as

$$N(\omega) = -\frac{1}{\pi} \text{Tr} \sum_{\mathbf{k}} \text{Im} G_{\alpha\beta}(\mathbf{k}, i\omega_n = \omega + i\delta), \quad (18)$$

where $G_{\alpha\beta}(\mathbf{k}, i\omega_n)$ is defined in Eq. (9). Features of the QDOS shown in Fig. 6 could be measured, in principle, during STM or photoemission experiments, depending on experimental resolution and material surface cleanliness. (In the case of photoemission, radiation damage due to X-rays, can also be an issue). Although, to our

knowledge, these experiments have not yet been successfully performed in $(\text{TMTSF})_2\text{ClO}_4$ and $(\text{TMTSF})_2\text{PF}_6$, our discussion can serve as qualitative guides for the extraction of gaps and symmetry dependent features of the experimental results when they become available. In particular, STM or photoemission measured gaps could be compared with gaps measured thermodynamically (e.g., thermal conductivity¹¹ or specific heat). However, a note of caution is in place here. Due to the expected unconventionality of quasi-one-dimensional superconductors, surface quasiparticle bound states could be present in these systems. The presence of these surface quasiparticle bound states was first noticed by Buchholtz and Zwickangl (BZ)⁴⁴ in isotropic p -wave superconductors and by Hu⁴⁵ in layered d -wave superconductors. Recently, Sengupta *et. al.*⁴⁶ followed the ideas of BZ⁴⁴ and Hu⁴⁵ and discussed the existence of these surface quasiparticle bound states in quasi-one-dimensional superconductors. The QDOS that we discuss is a bulk property, thus the contribution of these surface states is not reflected in our calculated QDOS.

We show in Fig. 5 the bulk QDOS at $T = 0$ K, and $T = 1$ K for the singlet states $^1A_{1g}$ (“s-wave”) and $^1B_{1g}$ (“ d_{xy} -wave”) as references. While in Fig. 6 we present the QDOS at $T = 0$ K and $T = 1$ K, with $T_c = 1.5$ K, for the states $^3B_{3u}(a)$ (weak spin-orbit coupling) and A_{1u}

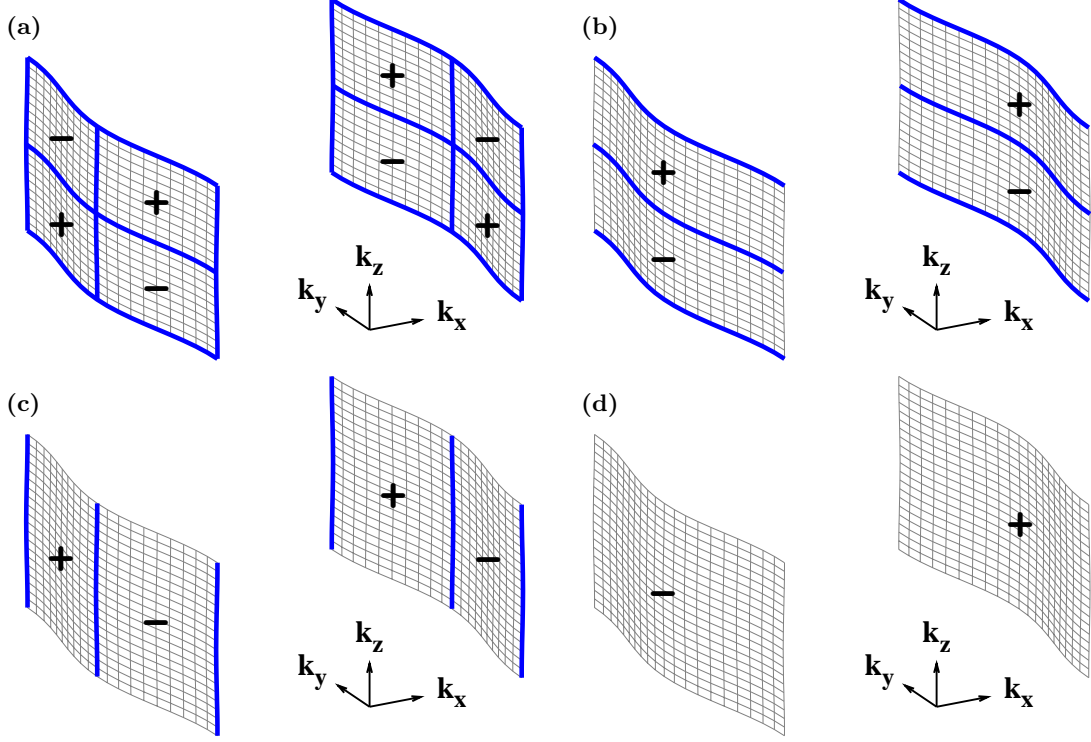


FIG. 2: Three dimensional views of the sign of the orbital component of the \mathbf{d} -vectors. Various weak spin-orbit coupling order parameter symmetries are illustrated (See Table IV): (a) ${}^3A_{1u}(a)$ (“ f_{xyz} -wave”); (b) ${}^3B_{1u}(a)$ (“ p_z -wave”); (c) ${}^3B_{2u}(a)$ (“ p_y -wave”); (d) ${}^3B_{3u}(a)$ (“ p_x -wave”). The thick lines correspond to the zeros of the orbital parts of the \mathbf{d} -vectors as well as to the excitation energy node structure ($E_{\mathbf{k}} = 0$) on the Fermi surface ($\tilde{\mu} > 0$).

(strong spin-orbit coupling) for various values of the constants A , B , and C . These constants reflect the strength and the anisotropy of the pairing interaction $V_{\alpha\beta\gamma\delta}(\mathbf{k}, \mathbf{k}')$ defined in Eq. 7 for the strong spin-orbit coupling case. The symmetry dependent features of the QDOS are manifested through the magnitude of the order parameter vector $\mathbf{d}(\mathbf{k})$. For the ${}^3B_{3u}(a)$ state the magnitude of $\mathbf{d}(\mathbf{k})$ is

$$|\mathbf{d}(\mathbf{k})| \propto |\sin(k_x a)|, \quad (19)$$

while for the A_{1u} state it takes the form $|\mathbf{d}(\mathbf{k})|$

$$\propto \sqrt{A^2 |\sin(k_x a)|^2 + B^2 |\sin(k_y b)|^2 + C^2 |\sin(k_z c)|^2}. \quad (20)$$

In Fig. 6(b), (c) and (d) we show only the case corresponding to $C = 0$, where $A \gg B$, $A = B$, and $A \ll B$, respectively. Notice that Fig. 6(d) is nearly identical to Fig. 6(a) given that $|\mathbf{d}(\mathbf{k})|$ is essentially the same in this case. Furthermore, notice that while the position of the peaks in Figs. 6(a), (b), (c) and (d) are essentially the same ($\omega_p \approx \pm 5.3$ K), the corresponding gap sizes are respectively $\omega_g = 2.27$ K; 0.29 K; 1.59 K; 2.27 K. In Fig. 7 we show the frequency dependence near the gap edge at $T = 0$ for the ${}^3B_{3u}(a)$ (weak spin-orbit coupling) state indicated in Fig. 6(a). The characteristic shape exhibited

here can also be found in the gapped states A_{1u} shown in Fig. 6(b), (c), and (d). In addition, the frequency dependence near the gap edge in these states obeys a square-root power law.

Although STM measures current (I) versus voltage (V) characteristics and not QDOS, the I - V (or dI/dV) characteristic are related to the QDOS. In a STM experiment one has to consider also the contribution of surface bound states, specially at zero voltage bias where a large contribution is expected in some cases^{44,45,46}. However, gap sizes, finite energy peaks and the general shape of the bulk QDOS should be, in principle, identifiable in an STM experiment at finite voltage bias.

It is also desirable to have photoemission experiments probing QDOS in the superconducting state of $(\text{TMTSF})_2\text{ClO}_4$ and $(\text{TMTSF})_2\text{PF}_6$, however the surfaces and the bulk of these materials seem to be very sensitive to X-rays. Thus, it is possible that photoemission may be not able to probe the QDOS without introducing disorder at the surface and the bulk of these materials. Even if STM and photoemission experiments could be successfully performed, these experiments alone cannot uniquely determine the symmetry of the order parameter in triplet quasi-one-dimensional superconductors since the QDOS depends only on the magnitude of $\mathbf{d}(\mathbf{k})$. Therefore, we now turn our attention to the calculation

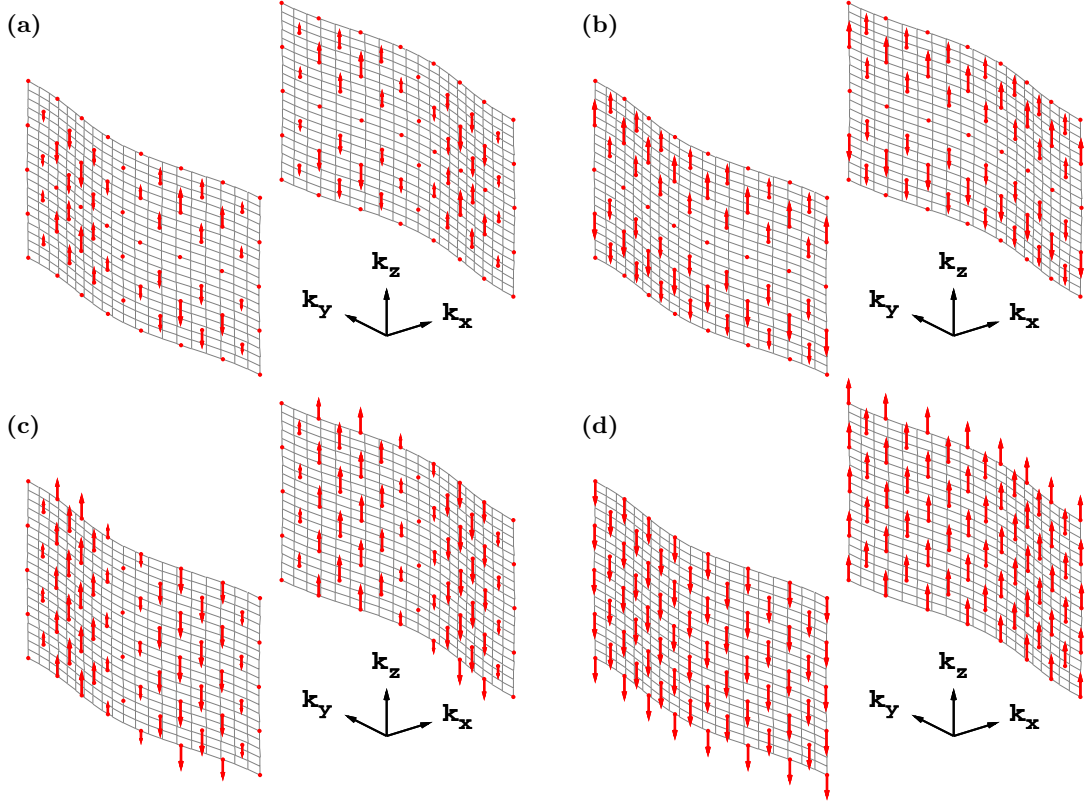


FIG. 3: Three dimensional views of \mathbf{d} -vectors at the Fermi surface ($\tilde{\mu} > 0$) for various weak spin-orbit coupling order parameter symmetries (See Table IV): (a) ${}^3A_{1u}(a)$ (“ f_{xyz} -wave”); (b) ${}^3B_{1u}(a)$ (“ p_z -wave”); (c) ${}^3B_{2u}(a)$ (“ p_y -wave”); (d) ${}^3B_{1u}(a)$ (“ p_x -wave”). For definiteness the \mathbf{d} -vectors are chosen to point along the \mathbf{c} direction.

of the spin susceptibility tensor, which explicitly depends both on the magnitude and direction of $\mathbf{d}(\mathbf{k})$.

V. SPIN SUSCEPTIBILITY

We obtain a general form of the spin susceptibility tensor given by

$$\chi_{mn}(q_\mu) = -\mu_B^2 (P_{mn})_{\alpha\beta\gamma\delta} [S_{\alpha\beta\gamma\delta}(q_\mu) + A_{\alpha\beta\gamma\delta}(q_\mu)], \quad (21)$$

where we used Einstein’s notation that repeated Greek indices indicate summation, and the four-vector $q_\mu = (\mathbf{q}, i\nu)$. The tensor

$$(P_{mn})_{\alpha\beta\gamma\delta} = \tilde{g}_m \tilde{g}_n (\sigma_m)_{\alpha\beta} (\sigma_n)_{\gamma\delta}, \quad (22)$$

contains the Pauli spin matrices and the scaled gyromagnetic factors $\tilde{g}_\ell = g_\ell/2$. The index ℓ takes into account the possibility of anisotropies in the gyromagnetic factors due to spin-orbit coupling. The other two tensors that appear in Eq. 21 are

$$A_{\alpha\beta\gamma\delta}(\mathbf{q}, i\omega) = \beta^{-1} \sum_{\mathbf{k}, i\omega} F_{\alpha\gamma}^\dagger(\mathbf{k} - \mathbf{q}, i\nu - i\omega) F_{\beta\delta}(\mathbf{k}, i\omega), \quad (23)$$

$$S_{\alpha\beta\gamma\delta}(q_\mu) = \beta^{-1} \sum_{\mathbf{k}, i\omega} G_{\delta\alpha}(-\mathbf{k} + \mathbf{q}, -i\nu + i\omega) G_{\beta\gamma}(\mathbf{k}, i\omega) \delta_{\delta\alpha} \delta_{\beta\gamma}, \quad (24)$$

which contain the Green’s functions described in Eqs. (8) and (9), respectively. In the limit of $\omega \rightarrow 0$ and

$\mathbf{q} \rightarrow \mathbf{0}$, we obtain an expression for the spin susceptibility of a triplet superconductor (including lattice and

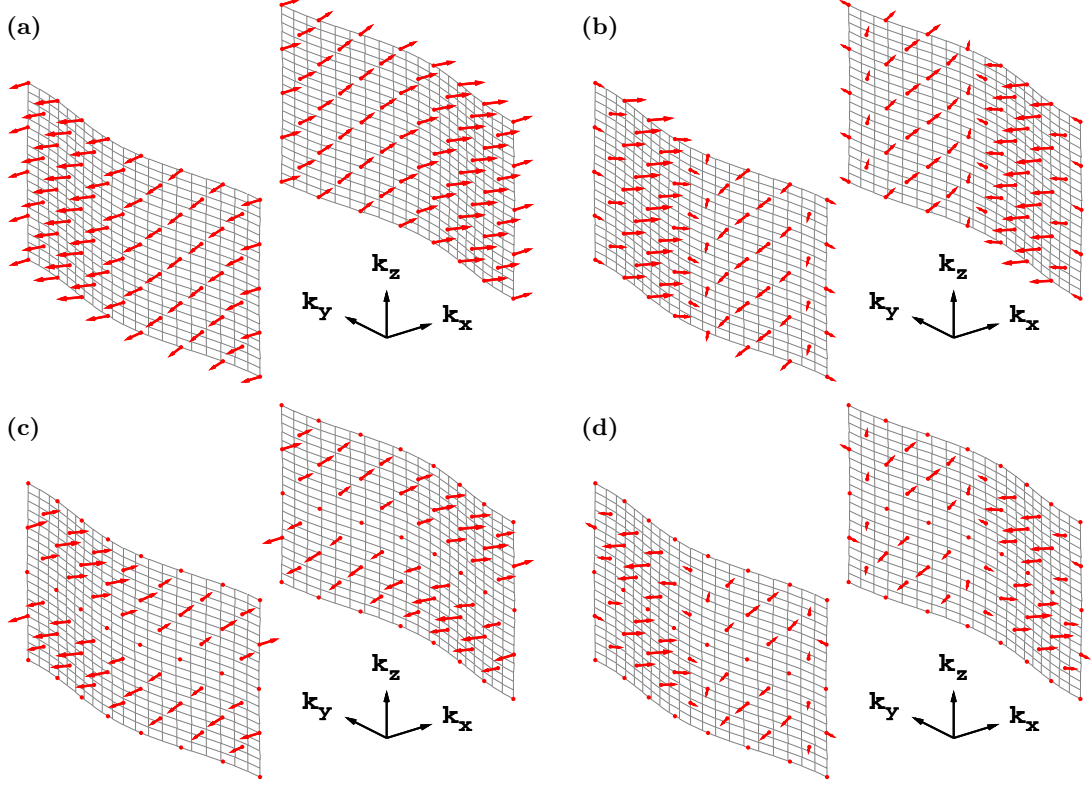


FIG. 4: Three dimensional views of \mathbf{d} -vectors at the Fermi surface ($\tilde{\mu} > 0$) for various strong spin-orbit coupling order parameter symmetries (See Table V): (a) A_{1u} ; (b) B_{1u} ; (c) B_{2u} ; (d) B_{1u} , for $A = B = 1$, and $C = 0$. Notice that the direction of the \mathbf{d} -vectors change along the Fermi surface, thus producing a textured structure.

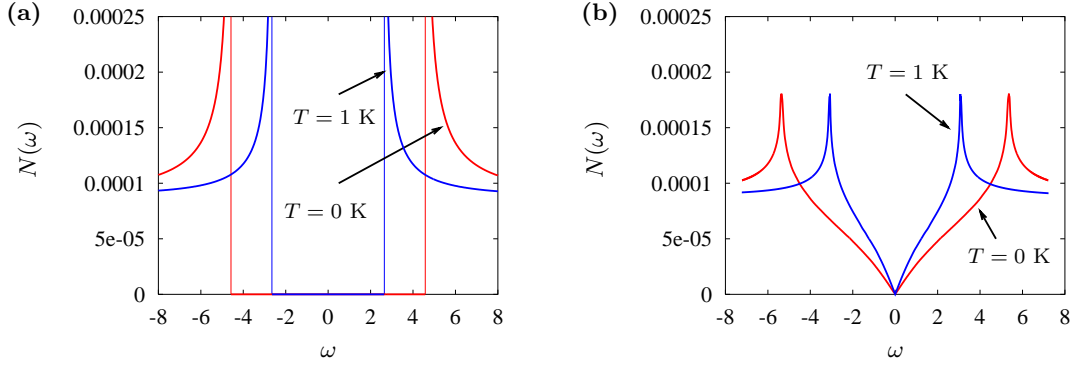


FIG. 5: The frequency dependence of the QDOS $N(\omega)$ for singlet symmetries at $T = 0$ K and $T = 1$ K. States $^1A_{1g}$ ("s-wave") and $^1B_{1g}$ ("dxy-wave") are shown respectively in (a) and (b). The parameters used are $|t_x| = 5800$ K, $|t_y| = 1226$ K, $|t_z| = 48$ K, and $\mu = -4101$ K, with $T_c = 1.5$ K. $N(\omega)$ is in inverse temperature units (K^{-1}) and ω is in temperature units (K).

particle-hole asymmetry effects),

$$\chi_{mn}(\mathbf{0}, 0) = \sum_{\mathbf{k}} [\chi_{mn,1}(\mathbf{k}) + \chi_{mn,2}(\mathbf{k})], \quad (25)$$

where the \mathbf{k} -dependent tensors have the forms

$$\chi_{mn,1}(\mathbf{k}) = \tilde{g}_m \tilde{g}_n \chi_{\parallel}(\mathbf{k}) \text{Re } \hat{d}_m^*(\mathbf{k}) \hat{d}_n(\mathbf{k}), \quad (26)$$

$$\chi_{mn,2}(\mathbf{k}) = \tilde{g}_m \tilde{g}_n \chi_{\perp}(\mathbf{k}) \left(\delta_{mn} - \text{Re } \hat{d}_m^*(\mathbf{k}) \hat{d}_n(\mathbf{k}) \right), \quad (27)$$

with $\hat{d}_n(\mathbf{k}) = d_n(\mathbf{k})/|d_n(\mathbf{k})|$. Here, the parallel component is

$$\chi_{\parallel}(\mathbf{k}) = -2\mu_B^2 \frac{\partial f(E_{\mathbf{k}})}{\partial E_{\mathbf{k}}}, \quad (28)$$

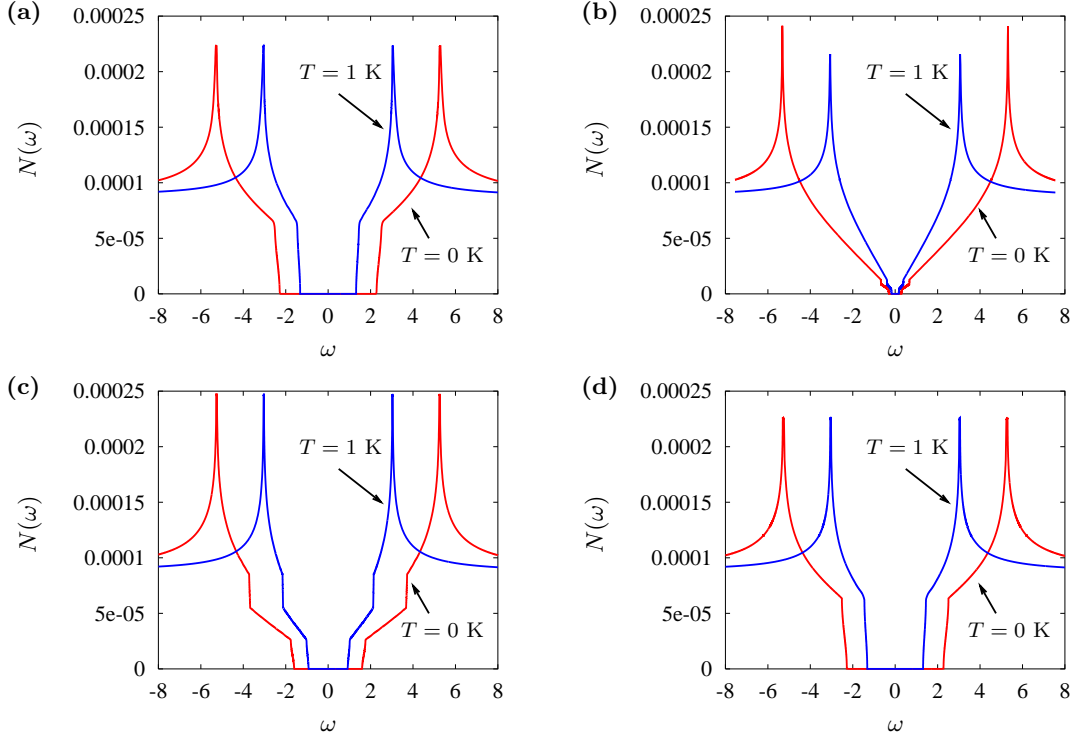


FIG. 6: Frequency dependence of the QDOS $N(\omega)$ for triplet states at $T = 0$ K and $T = 1$ K. In (a) the weak spin-orbit coupling state ${}^3B_{3u}$ is shown. In (b) strong spin-orbit coupling state A_{1u} is shown for $A = 0.20$, $B = 1.40$, $C = 0$; in (c) for $A = 1.00$, $B = 1.00$, $C = 0$; in (d) for $A = 1.41$, $B = 0.10$, $C = 0$. The parameters used are $|t_x| = 5800$ K, $|t_y| = 1226$ K and $|t_z| = 48$ K, and $\mu = -4101$ K, with $T_c = 1.5$ K. $N(\omega)$ is in inverse temperature units (K^{-1}) and ω is in temperature units (K).

while the perpendicular component is

$$\chi_{\perp}(\mathbf{k}) = 2\mu_B^2 \frac{d}{d\xi_{\mathbf{k}}} \left[\frac{\xi_{\mathbf{k}}}{2E_{\mathbf{k}}} (1 - 2f(E_{\mathbf{k}})) \right]. \quad (29)$$

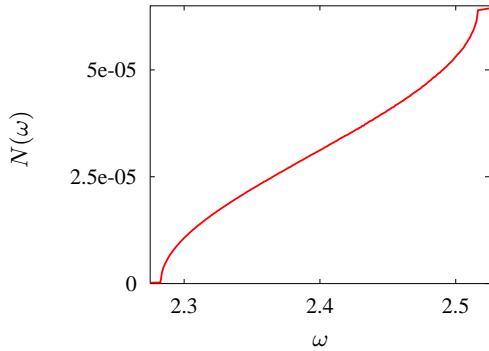


FIG. 7: A closer view of the $T = 0$ curve in Fig. 6(a) showing the frequency dependence of the QDOS $N(\omega)$ near the gap edge for the ${}^3B_{3u}$ state. This feature extends over an energy range of about 0.20 K ($17 \mu\text{eV}$). $N(\omega)$ is in inverse temperature units (K^{-1}) and ω is in temperature units (K).

The expressions derived in Eqs. (25) to (29) include some particle-hole symmetry effects, and are valid at all temperatures, within the BCS limits. They do not include, however, standard Fermi liquid corrections⁴⁷, since these corrections are expected to be small for $(\text{TMTSF})_2\text{PF}_6$ at lower pressures (near the SDW phase). In this pressure regime this compound behaves like a good Fermi liquid. However, the same can not be said at higher pressures, where deviations from standard Fermi liquid behavior were reported⁴⁸. The expression for $\chi_{mn}(\mathbf{0}, 0)$ in Eq. (25) also allows for anisotropies in the scaled gyromagnetic factors \tilde{g}_{ℓ} , where $\ell = m, n$. For instance, these anisotropies could already exist in the normal state of the system. Thus, it is important to measure experimentally such anisotropies to determine the strength of the spin-orbit coupling in the normal state. For the D_{2h} orthorhombic group χ_{mn} is diagonal, but in the presence of spin-orbit coupling the normal state $\chi_{mn}^{(N)}$ can have, in principle, all diagonal elements different from each other i.e., $\chi_{11}^{(N)} \neq \chi_{22}^{(N)} \neq \chi_{33}^{(N)} \neq \chi_{11}^{(N)}$. In the complete absence of spin-orbit coupling $\tilde{g}_{\ell} = 1$ for all ℓ , and $\chi_{11}^{(N)} = \chi_{22}^{(N)} = \chi_{33}^{(N)} = \chi_N$.

In Fig. 8, the theoretical uniform χ_{mn} is shown only for the ${}^3B_{3u}$ and A_{1u} states. We do not discuss other strong spin-orbit coupling states B_{1u} and B_{2u} , which can also

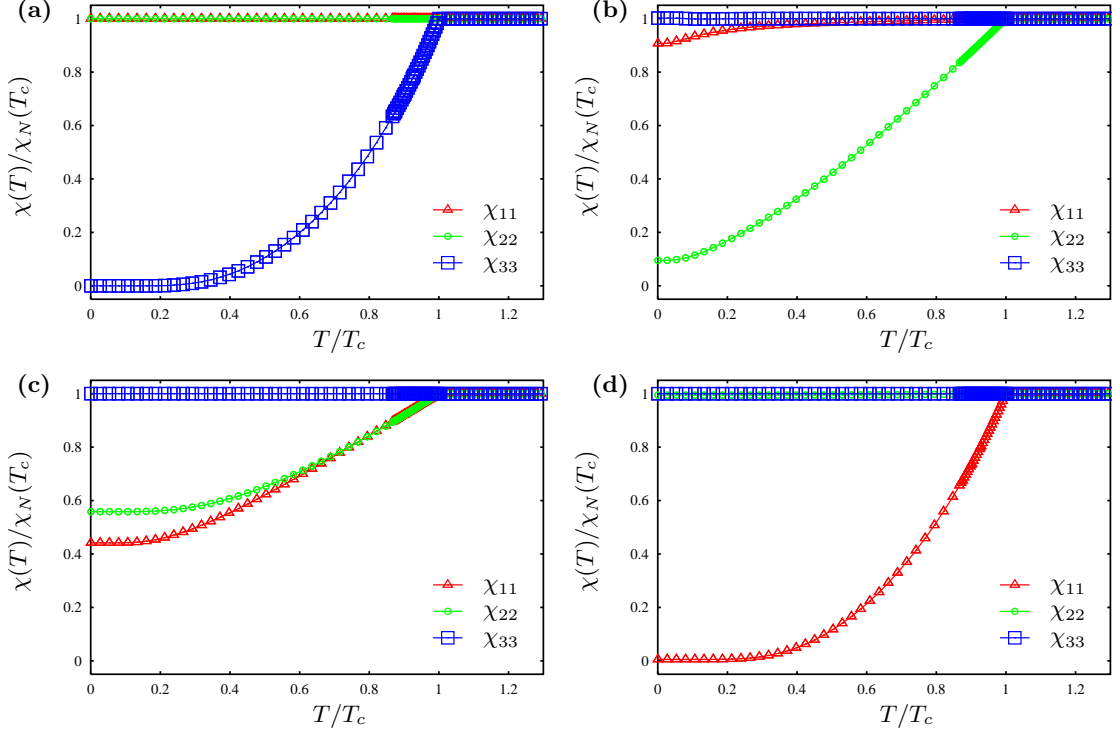


FIG. 8: Plot of the theoretical uniform spin susceptibility tensor components χ_{11} (triangles); χ_{22} (circles); χ_{33} (squares) at low temperatures. The weak spin-orbit coupling state ${}^3B_{3u}$ is shown in (a); strong spin-orbit coupling state A_{1u} is shown in (b) for $A = 0.20$, $B = 1.40$, $C = 0$; in (c) for $A = 1.00$, $B = 1.00$, $C = 0$; in (d) for $A = 1.41$, $B = 0.10$, $C = 0$. The parameters used are $|t_x| = 5800$ K, $|t_y| = 1226$ K, $|t_z| = 48$ K, and $\mu = -4101$ K, with $T_c = 1.5$ K.

be fully gapped because the atomic spin-orbit coupling in Bechgaard salts seems to be small (Se is the heaviest element). The triangles correspond to χ_{11} circles to χ_{22} , and squares to χ_{33} . The susceptibilities χ_{mn} are scaled by their normal state values $\chi_{mn}^{(N)}$. It is known experimentally (Knight shift)⁵ that the spin susceptibility of (TMTSF)₂PF₆ for $\mathbf{H} \parallel \mathbf{b}'$ ($H = 2.38$ T) is very close to $\chi_{b'}^{(N)}$. Knight shift experiments with $\mathbf{H} \parallel \mathbf{a}^6$ ($H = 1.34$ T) also indicate that the spin susceptibility is very close to $\chi_a^{(N)}$. However if experiments indicate that the normal state susceptibilities obey the relation $\chi_a^{(N)} \approx \chi_{b'}^{(N)} \approx \chi_{c^*}^{(N)} \approx \chi_N$, then this is strongly suggestive that spin-orbit coupling effects are small, as expected from the fact that (TMTSF)₂ClO₄ and (TMTSF)₂PF₆ have reasonably light atoms. Furthermore, in recent experiments, Lee *et al.*⁶ observed a coherence peak in the NMR relaxation rate $1/T_1$ for $\mathbf{H} \parallel \mathbf{a}$, $H = 1.43$ T. In conventional superconductors the enhancement of $1/T_1$ near T_c is often associated with a divergence of the density of states at the edge of the energy gap⁷. Although the weak spin-orbit coupling fully gapped state ${}^3B_{3u}(a)$ (“ p_x -wave”) (see Fig. 6) does not exhibit a divergence in QDOS at the edge of the energy gap, the QDOS changes very rapidly at the edge and may produce a peak or a kink in $1/T_1$ for ${}^{77}\text{Se}$.

These results reinforce the evidence for triplet superconductivity in (TMTSF)₂PF₆. For fields along the \mathbf{c}^* direction the superconducting state is easily destroyed, which makes impractical the Knight shift measurement for ${}^{77}\text{Se}$. This measurement requires magnetic fields of the order of one Tesla, which is an order of magnitude higher than the upper critical field along this direction⁴. For definiteness, we choose the unit vectors $\hat{1}$ ($m = 1$), $\hat{2}$ ($m = 2$) and $\hat{3}$ ($m = 3$), to point along the \mathbf{a} , \mathbf{b}' , and \mathbf{c}^* directions, respectively.

A. Finite Magnetic Field Effects

In this section, we discuss qualitatively some of the effects of a finite magnetic field upon the spin susceptibility tensor. We consider first the effects of vortices on the spin susceptibility tensor within a simple two fluid model, and second the possible rotation of the \mathbf{d} -vector in the presence of a finite magnetic field.

1. Role of Vortices

Here, we would like to comment on the role of vortices when the spin susceptibility tensor is measured.

The Knight shift measurements of Lee *et. al.*^{5,6} in (TMTSF)₂PF₆ had to be performed at reasonably high fields $H = 2.38$ T for $\mathbf{H} \parallel \mathbf{b}$ and $H = 1.43$ T for $\mathbf{H} \parallel \mathbf{a}$ in order to obtain a clear NMR signal. In these field regimes the superconductor (TMTSF)₂PF₆ is in an inhomogeneous vortex state. This vortex state was analysed by DMS²⁰, and later shown by Sá de Melo²⁴ to correspond to a rectangular Abrikosov vortex lattice (in the semiclassical low field regime) and to a rectangular Josephson vortex lattice (in the quantum high field regime) for equal spin triplet pairing or singlet pairing. We will use this result to construct a simple phenomenological two-fluid model to describe the effect of vortices on the spin susceptibility tensor, while a more sophisticated calculation is under way⁴⁹. Let us consider our superconductor at finite T and H , and assume a semiclassical description of the vortex state. Assume that the magnetic field is applied along the \hat{n} direction ($H_{\hat{n}}$) and produces a rectangular Abrikosov lattice with lattice constants $\ell_{\hat{\alpha}}$ and $\ell_{\hat{\beta}}$, where $\hat{\alpha}$ and $\hat{\beta}$ are direction perpendicular to \hat{n} . The density of vortices is $n_v = 1/\ell_{\hat{\alpha}}\ell_{\hat{\beta}}$. Assuming that the vortices have finite core size, characterized by lengths $\xi_{\hat{\alpha}}$ and $\xi_{\hat{\beta}}$, and that the vortex core is normal⁵⁰, the normal fraction of the superconductor is

$$n_f = \frac{\xi_{\hat{\alpha}}\xi_{\hat{\beta}}}{\ell_{\hat{\alpha}}\ell_{\hat{\beta}}} = \frac{H_{\hat{n}}}{H_{c2\hat{n}}} \quad (30)$$

Vortex core states have been extensively investigated in singlet superconductors^{51,52,53,54,55,56,57,58,59}; however, these states in triplet superconductors remain to be investigated⁵⁰. We treat core states very crudely as nearly *particle-in-a-well*-like with characteristic sizes controlled by the coherence lengths $\xi_{\hat{\alpha}}$, and $\xi_{\hat{\beta}}$ transverse to the magnetic field direction. This is a crude improvement upon treating vortex cores as purely normal, while a more sophisticated calculation of vortex core states is under way⁴⁹. In the present case, if the two fluids are viewed as nearly independent⁶⁰, then the total spin susceptibility tensor of the superconductor is the sum of the response of its individual components. Thus, we write

$$\chi_{mn}(T, H_{\hat{n}}) = \chi_{mn}^{(C)}(T, H_{\hat{n}})n_f + \chi_{mn}^{(S)}(T, H_{\hat{n}})(1 - n_f), \quad (31)$$

where $\chi_{mn}^{(C)}(T, H_{\hat{n}})$ is the vortex core contribution, and $\chi_{mn}^{(S)}(T, H_{\hat{n}})$ is the superconducting contribution. However it is best to illustrate the qualitative behavior of $\chi_{mn}(T, H_{\hat{n}})$ via the ratio

$$R(T, H_{\hat{n}}) = R_C(T, H_{\hat{n}})n_f + R_S(T, H_{\hat{n}})(1 - n_f) \quad (32)$$

Here $R(T, H_{\hat{n}}) \equiv \chi_{mn}(T, H_{\hat{n}})/\chi_{mn}^{(N)}(T, H_{\hat{n}})$, and $R_j(T, H_{\hat{n}}) \equiv \chi_{mn}^{(j)}(T, H_{\hat{n}})/\chi_{mn}^{(N)}(T, H_{\hat{n}})$, with $j = C, S$. In Fig. 9a the ratio $R(T, H_{\hat{n}})$ for a weak spin-orbit coupling triplet superconductor is illustrated for fixed temperature $T < T_c$. It is assumed that the applied magnetic field is perpendicular to the \mathbf{d} -vector ($\mathbf{H} \perp \mathbf{d}$),

and that \mathbf{d} -vector direction is not affected by the magnetic field. In this case, $0 \leq R_C(T, H_{\hat{n}}) \leq 1$, such that $R_C(T, H_{\hat{n}})$ changes from a smaller value at small n_f at fixed temperature, and as n_f tends to 1, $R_C(T, H_{\hat{n}})$ converges to 1, given that the core spectrum becomes the normal state continuum at $H_{\hat{n}} = H_{c2\hat{n}}$. The superconducting term is assumed to be essentially constant for ($\mathbf{H} \perp \mathbf{d}$), and $R_S(T, H_{\hat{n}}) \approx 1$, implying that the total ratio $R(T, H_{\hat{n}}) \approx 1$. These results are largely independent of temperature and field within the approximation used. However, the discussion above serves only as a qualitative guide, while a more sophisticated analysis is under way⁴⁹. In Fig. 9b the qualitatively similar situations of a weak spin-orbit coupling singlet superconductor or weak spin-orbit coupling triplet superconductor with $\mathbf{H} \parallel \mathbf{d}$ are illustrated. In this case, the core term $R_C(T, H_{\hat{n}})$ still satisfies the condition $0 \leq R_C(T, H_{\hat{n}}) \leq 1$, and grows at fixed temperature from a smaller value at small n_f to $R_C(T, H_{\hat{n}}) = 1$ as n_f tends to 1. In addition, the contribution of the superconducting part $R_S(T, H_{\hat{n}})$ depends strongly on magnetic field (at fixed temperature) growing from a small value at small n_f to $R_S(T, H_{\hat{n}}) = 1$ as $n_f \rightarrow 1$. The condition $0 \leq R_S(T, H_{\hat{n}}) \leq 1$ is also satisfied. Therefore, $R(T, H_{\hat{n}})$ would be very strongly dependent on magnetic field (at fixed temperature) in (a) the weak spin-orbit triplet case for $\mathbf{H} \parallel \mathbf{d}$, or in (b) the weak spin-orbit singlet case. Thus, if measurements of temperature and magnetic field dependence of $\chi_{mn}(T, H_{\hat{n}})$ in (TMTSF)₂PF₆ are such that $R_S(T, H_{\hat{n}}) \approx 1$ (being largely independent of magnetic field at fixed temperature), then a weak spin-orbit triplet state would be consistent with such finding for $\mathbf{H} \perp \mathbf{d}$. It is possible, however, that a small magnetic field can rotate the \mathbf{d} -vector in the weak spin-orbit coupling limit, and this effect is discussed next.

2. Rotation of \mathbf{d} -vector

In what follows, we will discuss the possible rotation of $\mathbf{d}(\mathbf{k})$, not including vortex core contributions, i.e., we will consider effectively only $\chi_{mn}^{(S)}(T, H_{\hat{n}})$. However, similar effects are expected for the core contribution.

For the orthorhombic symmetry χ_{mn} is diagonal and is calculated under the assumption that $\mathbf{d}(\mathbf{k})$ is constant, i.e., the direction of $\mathbf{d}(\mathbf{k})$ is assumed not to change upon the application of a small magnetic field. In the case of state A_{1u} (strong spin-orbit coupling) a small magnetic field cannot rotate $\mathbf{d}(\mathbf{k})$ which is pinned to a particular lattice direction. In the strong spin-orbit coupling case χ_{mn} is still diagonal, however the diagonal components are not equal in general. Thus, the experimentally measured χ_{mn}^{ex} and the theoretically calculated χ_{mn}^{th} (at constant $\mathbf{d}(\mathbf{k})$) should agree for small enough magnetic fields (see Fig. 8b 8c, and 8d). However, in the case of state $^3B_{3u}(a)$ (weak spin-orbit coupling) a small magnetic field can easily rotate $\mathbf{d}(\mathbf{k})$ to be perpendicular to \mathbf{H} (barring any additional orbital effects due to the coupling

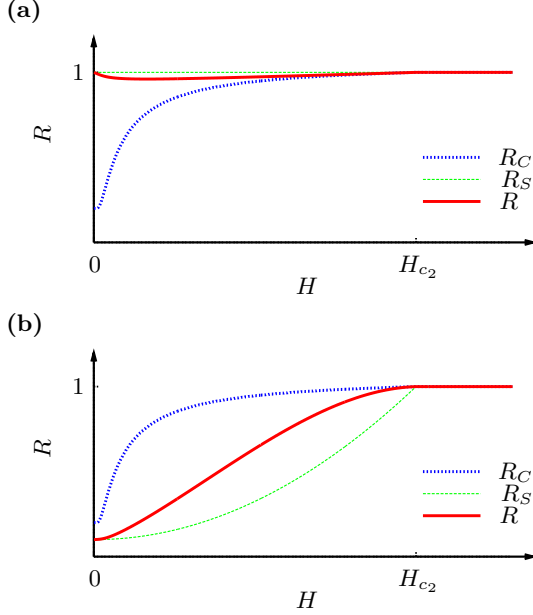


FIG. 9: Schematic plots of the ratios R (solid line); R_C (dashed line); and R_S (dotted line) are shown in (a) for the case of a weak spin-orbit coupling triplet superconductor with $\mathbf{H} \perp \mathbf{d}$; and in (b) for the case of a weak spin-orbit coupling singlet superconductor or weak spin-orbit coupling triplet superconductor with $\mathbf{H} \parallel \mathbf{d}$. The ratio R is connected to R_C and R_S via Eq. 32. (See text following Eq. 32 for definition of ratios R , R_C and R_S .)

of \mathbf{H} with charge degrees of freedom), thus minimizing the magnetic free-energy $F_{mag} = -H_m \chi_{mn} H_n / 2$. In the weak spin-orbit coupling case, $\chi_{mn}^{ex} \approx \chi_N \delta_{mn}$, where χ_N is the normal state value, for any direction of \mathbf{H} . Thus, what experimentalists measure, χ_{mn}^{ex} , and what we calculate, χ_{mn}^{th} , (shown in Fig. 8a) would be different. (This point was considered by Leggett⁴⁷ in his discussion of the phases of liquid ^3He). Another important distinguishing feature between strong spin-orbit and weak spin-orbit coupling scenarios is the magnitude of the flop field H_f required to rotate the \mathbf{d} -vector from a preferred lattice direction. In the case of strong spin-orbit coupling the flop fields are in the Tesla range, while for weak spin-orbit coupling the flop fields are in the Gauss range. For instance, based on the discussion above, the state $^3B_{3u}(a)$ (weak spin-orbit coupling “ p_x -wave”) would present no Knight shift for any direction of the externally applied magnetic field provided that the magnitude of \mathbf{H} is larger than the small spin-orbit pinning field H_f for any given direction. Under these conditions, no Knight shift should be observed for fields along the \mathbf{a} , \mathbf{b}' or \mathbf{c}^* -axis or for any set of angles with respect to these axis. Furthermore, in the weak spin-orbit coupling state $^3B_{3u}(a)$ (“ p_x -wave”), the normal state susceptibilities should be nearly identical, i.e. $\chi_{11}^{(N)} \approx \chi_{22}^{(N)} \approx \chi_{33}^{(N)} = \chi_N$, since the scaled gyromagnetic factors $\tilde{g}_\ell \approx 1$ for all ℓ .

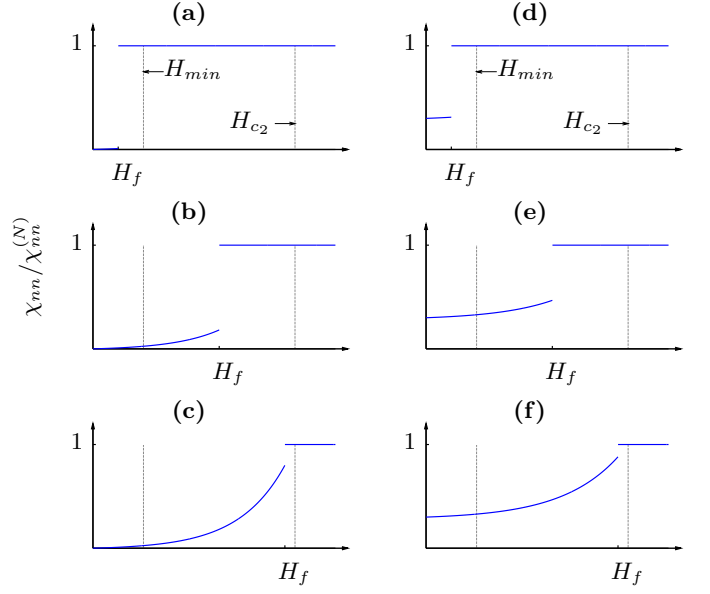


FIG. 10: Scenarios for the behavior of the experimental $\chi_{nn}/\chi_{nn}^{(N)}$ considering that the \mathbf{d} -vector is pinned along the \hat{n} direction. The ratio $\chi_{nn}/\chi_{nn}^{(N)}$ is schematically plotted as a function of applied magnetic field at a constant $T = 0$ (left set) and $T > 0$ (right set). The lower upper critical field $H_{c1}^{(\hat{n})}$ is assumed to be very small and it is not shown. In each of these graphs, the left and right vertical dotted lines represent the minimum field ($H_{min}^{(\hat{n})}$) required to obtain Knight shift experimental data and the upper critical field ($H_{c2}^{(\hat{n})}$) corresponding a fixed temperature T . Three possible flop transition scenarios at $T = 0$: (a) $H_f^{(\hat{n})} < H_{min}^{(\hat{n})} < H_{c2}^{(\hat{n})}$ (flop transition beyond present experimental reach); (b) $H_{min}^{(\hat{n})} < H_f^{(\hat{n})} < H_{c2}^{(\hat{n})}$ (flop transition can be observed if jump in susceptibility is large enough); (c) $H_{min}^{(\hat{n})} < H_f^{(\hat{n})} \lesssim H_{c2}^{(\hat{n})}$ (flop transition may be difficult to be observed since jump in susceptibility may be too small). Similar scenarios are illustrated in (d), (e) and (f) for $T > 0$.

The spin susceptibility tensor for a triplet superconductor is very sensitive to magnetic fields both in the weak or strong spin-orbit coupling scenarios since the applied field can depin the \mathbf{d} -vector from a preferred lattice direction and cause a flop transition with a corresponding change in the spin susceptibility. This means that with increasing magnetic field at fixed temperature T , $H > H_{c1}$, and with $\mathbf{H} \parallel \mathbf{d}$ initially, the \mathbf{d} -vector flops at $H = H_f < H_{c2}$. Therefore, beyond H_f the \mathbf{d} -vector becomes perpendicular to the applied magnetic field ($\mathbf{d} \perp \mathbf{H}$). This flop transition produces a discontinuous change in the spin susceptibility from smaller to larger (normal) values, as the \mathbf{d} -vector rearranges itself from $\mathbf{d} \parallel \mathbf{H}$ to $\mathbf{d} \perp \mathbf{H}$.

Consider for definiteness that the \mathbf{d} -vector is pinned along a given lattice direction \hat{n} , and that $\mathbf{H} \parallel \mathbf{d}$. The observability of this flop transition depends on how the magnitude $H_f^{(\hat{n})}$ compares to the magnitudes of the min-

imum field required to perform a Knight shift experiment, $H_{min}^{(\hat{n})}$, the lower $H_{c1}^{(\hat{n})}$ and the upper $H_{c2}^{(\hat{n})}$ critical fields along the given direction \hat{n} . Three possible scenarios are illustrated in Fig. 10, where $H_{c1}^{(\hat{n})}$ is considered to be very small and it is not indicated in the figure. If $H_f^{(\hat{n})} \ll H_{min}^{(\hat{n})}$ then the transition cannot be observed in a Knight shift experiment. If $H_f^{(\hat{n})} \lesssim H_{c2}^{(\hat{n})}$ then, depending on experimental resolution, the transition may not be resolvable and the data would seem characteristic of a singlet response. However, the flop transition could be easily measured in the intermediate regime $H_{min}^{(\hat{n})} < H_f^{(\hat{n})} < H_{c2}^{(\hat{n})}$. If \mathbf{d} was pinned along $\hat{n} = \mathbf{a}$, then for $\mathbf{H} \parallel \mathbf{a}$ such that $H > H_f^{(\mathbf{a})}$ a flop transition could take place. Similarly situations would occur if the \mathbf{d} -vectors were pinned along $\hat{n} = \mathbf{b}'$ (\mathbf{c}^*), then for $\mathbf{H} \parallel \mathbf{b}'$ (\mathbf{c}^*) such that $H > H_f^{(\mathbf{b}')} (H > H_f^{(\mathbf{c}^*)}$ a flop transition could take place. So far there is no experimental evidence of this possible \mathbf{d} -vector flop transition.

3. Connection to Anisotropy Inversion in H_{c2}

It is also important to make a connection between spin susceptibility measurements^{5,6} and upper critical field measurements⁴ in $(\text{TMTSF})_2\text{PF}_6$. Lee *et. al.*⁴ observed an anisotropy inversion between $H_{c2}^{(\mathbf{a})}$ and $H_{c2}^{(\mathbf{b}')}$ at $H^* \approx 1.6 T$. It was suggested theoretically³⁰ that this anisotropy inversion was related to the presence of a component of the \mathbf{d} -vector along the \mathbf{a} direction, such that $H_{c2}^{(\mathbf{a})}$ ($\mathbf{H} \parallel \mathbf{a}$) would be paramagnetically limited. In addition, it was suggested that³⁰ the \mathbf{d} -vector would have zero component along the \mathbf{b}' direction, such that $H_{c2}^{(\mathbf{b}')} (\mathbf{H} \parallel \mathbf{b}')$ would not be paramagnetically limited. While this suggestion is somewhat appealing, it seems to indicate that the \mathbf{d} -vector has a strongly pinned component along the \mathbf{a} axis.

A comparison between the upper critical field experiments of Lee *et. al.*⁴ for $(\text{TMTSF})_2\text{PF}_6$, with the upper critical field experiments of Shivaram *et. al.*⁶¹ for UPt_3 can be illuminating. In UPt_3 an anisotropy inversion occurs between the upper critical fields between $H_{c2}^{(\mathbf{a})}$ and $H_{c2}^{(\mathbf{c})}$ at $H^* \approx 1.9 T$. This anisotropy inversion in UPt_3 was successfully explained by Choi and Sauls⁶² under the assumption that $H_{c2}^{(\mathbf{c})}$ is paramagnetically limited, while $H_{c2}^{(\mathbf{a})}$ is not. The nearly perfect fitting of the experimental curves of UPt_3 required the assumption that the \mathbf{d} -vector was locked to the \mathbf{c} axis by a strong spin-orbit coupling. Considering that the values of the anisotropy inversion field H^* for $(\text{TMTSF})_2\text{PF}_6$ and UPt_3 are very similar in magnitude, the theoretical interpretation³⁰ of the anisotropy inversion in $(\text{TMTSF})_2\text{PF}_6$ seems to assume implicitly a strong spin-orbit coupling, which is very unlikely for Bechgaard salts given that the heaviest element is Se. The ratio r_{so} between (atomic) spin-orbit couplings in $(\text{TMTSF})_2\text{PF}_6$ (for Se) and UPt_3 (for U)

can be estimated to be small: $r_{so} \lesssim 0.15$. This implies that the physical origin of the anisotropy inversion in $(\text{TMTSF})_2\text{PF}_6$ should not be implicitly or explicitly the same as in UPt_3 . Furthermore, the theoretical suggestion connecting the anisotropy inversion with spin susceptibility measurements³⁰ would lead to $\chi_a \approx 0.2\chi_N$ at $T = 0$. However, experiments indicate that $\chi_a \approx \chi_N$ ⁶ in $(\text{TMTSF})_2\text{PF}_6$ ($T_c = 1.2 K$) down to $T = 0.32 K$.

It is important to note that the related compound $(\text{TMTSF})_2\text{AsF}_6$ has an SDW phase below $T_c = 12 K$ with easy, intermediate and hard axis along the \mathbf{b}' , \mathbf{a} , and \mathbf{c}^* directions, respectively⁶³. This system also presents a spin-flop transition where the spin orientation flops from the \mathbf{b}' axis to an orientation predominantly parallel to \mathbf{a} ⁶³. Given that the SDW phase in $(\text{TMTSF})_2\text{PF}_6$ is very similar to the SDW phase in $(\text{TMTSF})_2\text{AsF}_6$ ⁶³, we infer that the connection between the experimental results $\chi_a \approx \chi_N$ and $\chi_{b'} \approx \chi_N$ ^{5,6} with the anisotropy inversion of the upper critical fields $H_{c2}^{(\mathbf{a})}$ and $H_{c2}^{(\mathbf{b}')}$ in $(\text{TMTSF})_2\text{PF}_6$ may require a deeper understanding of the interplay between the spin-density-wave and the superconducting phases. Thus, it is important to search for an H_{c2} anisotropy inversion in the sister compound $(\text{TMTSF})_2\text{ClO}_4$ in order to have a more complete picture of the superconducting state in the Bechgaard salt family $(\text{TMTSF})_2\text{X}$. To our knowledge detailed experimental studies of $H_{c2}^{(\mathbf{a})}$ (high fields and low temperatures) have not yet been performed for $(\text{TMTSF})_2\text{ClO}_4$. Having made this last experimental connection, we are ready to summarize our results.

VI. SUMMARY

We performed a group theoretical analysis of the possible symmetries compatible with the D_{2h} (orthorhombic) point group, and focused on the weak and strong spin-orbit coupling triplet cases at zero magnetic field. We also discussed order parameter symmetry features and temperature dependence of the quasiparticle density of states and spin susceptibility tensor of an orthorhombic quasi-one-dimensional superconductor³⁷. Based on current experimental evidence and the assumption that the origin of superconductivity in $(\text{TMTSF})_2\text{ClO}_4$ and $(\text{TMTSF})_2\text{PF}_6$ is essentially the same, we suggested that the weak spin-orbit coupling state $^3B_{3u}(a)$ (" p_x -wave") is a very good candidate for the order parameter symmetry for these systems since this state is: (1) fully gapped and consistent with thermal conductivity measurements¹¹; (2) characterized by weak spin-orbit coupling and consistent with weak spin-orbit scattering fits of $T_c(H)$ for $(\text{TMTSF})_2\text{PF}_6$ ⁶⁴ at low magnetic fields; (3) consistent with no observable Knight shift when $\mathbf{H} \parallel \mathbf{a}$ ⁶ or $\parallel \mathbf{b}'$ ⁴, and predicted to have no observable Knight shift for any direction \hat{n} of \mathbf{H} provided that the magnitude of the applied field is larger than the small spin-orbit pinning field $H_f^{(\hat{n})}$. We would like to thank NSF (Grant No.

DMR-9803111) and its REU program for support. One of us (C. A. R. Sá de Melo) would like to thank the Aspen Center for Physics for its hospitality.

[†] Present address: Department of Physics, Massachusetts Institute of Technology, Cambridge, MA 02139-4307.

- ¹ D. Jerome, A. Mazaud, M. Ribault, and K. Bechgaard, J. Phys. Lett. **41**, L95 (1980).
- ² T. Ishiguro and K. Yamaji, *Organic Superconductors* (Springer-Verlag, 1989).
- ³ J. M. Williams, J. R. Ferraro, R. J. Thorn, K. G. Carlson, U. Geiser, H. H. Wang, A. M. Kini, and M. H. Whangbo, *Organic Superconductors (Including Fullerenes): Synthesis, Structure, Properties and Theory* (Prentice Hall, 1992).
- ⁴ I. J. Lee, M. J. Naughton, G. M. Danner, and P. M. Chaikin, Phys. Rev. Lett. **78**, 3555 (1997).
- ⁵ I. J. Lee, D. S. Chow, W. G. Clark, M. J. Strouse, M. J. Naughton, P. M. Chaikin, and S. E. Brown (2000), cond-mat/0001332.
- ⁶ I. J. Lee, S. E. Brown, W. G. Clark, M. J. Strouse, M. J. Naughton, W. Kang, and P. M. Chaikin, Phys. Rev. Lett. **88**, 017004 (2002).
- ⁷ L. C. Hebel and C. P. Slichter, Phys. Rev. **113**, 1504 (1959).
- ⁸ M. Takigawa, H. Yasuoka, and G. Saito, Journ. Phys. Soc. Japan **56**, 873 (1987).
- ⁹ I. J. Lee, A. P. Hope, M. J. Leone, and M. J. Naughton, Applied Superconductivity **2**, 753 (1994).
- ¹⁰ I. J. Lee, A. P. Hope, M. J. Leone, and M. J. Naughton, Synth. Metals **70**, 747 (1995).
- ¹¹ S. Belin and K. Behnia, Phys. Rev. Lett. **79**, 2125 (1997).
- ¹² D. A. Wollman, D. J. V. Harlingen, W. C. Lee, D. M. Ginsberg, and A. J. Leggett, Phys. Rev. Lett. **71**, 2134 (1993).
- ¹³ A. Mathai, Y. Gim, R. C. Black, A. Amar, and F. C. Wellstood, Phys. Rev. Lett. **74**, 4523 (1995).
- ¹⁴ A. A. Abrikosov, JETP Lett. **37**, 503 (1983).
- ¹⁵ A. A. Abrikosov, J. Low Temp. Phys. **53**, 359 (1983).
- ¹⁶ M. Y. Choi, P. M. Chaikin, S. Z. Huang, P. Haen, E. M. Engler, and R. L. Greene, Phys. Rev. B **25**, 6208 (1982).
- ¹⁷ S. Bouffard, M. Ribault, R. Brussetti, D. Jerome, and K. Bechgaard, J. Phys. C: Solid State Phys. **15**, 2951 (1982).
- ¹⁸ L. P. Gorkov and D. Jerome, J. Physique Lett. **46**, L643 (1985).
- ¹⁹ A. G. Lebed, Sov. Phys. JETP Lett. **44**, 89 (1986).
- ²⁰ N. Dupuis, G. Montambaux, and C. A. R. Sá de Melo, Phys. Rev. Lett. **70**, 2613 (1993).
- ²¹ A. I. Larkin and Y. N. Ovchinnikov, Sov. Phys. JETP **20**, 762 (1965).
- ²² P. Fulde and R. A. Ferrel, Phys. Rev. **135**, A550 (1964).
- ²³ N. Dupuis, Phys. Rev. B **51**, 9074 (1995).
- ²⁴ C. A. R. Sá de Melo, Physica C **260**, 224 (1996).
- ²⁵ A. G. Lebed, Phys. Rev. B **59**, R721 (1999).
- ²⁶ C. A. R. Sá de Melo, *The Superconducting State in Magnetic Fields: Special Topics and New Trends* (World Scientific, Singapore, 1998), chap. 15, pp. 296–324, (Edited by C. A. R. Sá de Melo).
- ²⁷ C. A. R. Sá de Melo, J. Supercond. **12**, 459 (1999).
- ²⁸ C. D. Vaccarella and C. A. R. Sá de Melo, Physica C **341-348**, 293 (2000).
- ²⁹ C. D. Vaccarella and C. A. R. Sá de Melo, Phys. Rev. B **63**, R180505 (2001).
- ³⁰ A. G. Lebed, K. Machida, and M. Ozaki, Phys. Rev. B **62**, R795 (2000).
- ³¹ H. Shimahara, Phys. Rev. B **61**, R14936 (2000).
- ³² K. Kuroki, R. Arita, and H. Aoki, Phys. Rev. B **63**, 094509 (2001).
- ³³ R. D. Duncan, C. D. Vaccarella, and C. A. R. Sá de Melo, Phys. Rev. B **64**, 172503 (2001).
- ³⁴ V. P. Mineev and K. V. Samokhin, *Introduction to Unconventional Superconductivity* (Gordon and Breach, Amsterdam, 1999).
- ³⁵ C. A. R. Sá de Melo, M. Randeria, and J. R. Engelbrecht, Phys. Rev. Lett. **71**, 3202 (1993).
- ³⁶ J. R. Engelbrecht, M. Randeria, and C. A. R. Sá de Melo, Phys. Rev. B **55**, 15153 (1997).
- ³⁷ The Bechgaard salts (TMTSF)₂ClO₄ and (TMTSF)₂PF₆ have truly a triclinic lattice structure.
- ³⁸ P. W. Anderson, Phys. Rev. B **30**, 4000 (1984).
- ³⁹ M. Tinkham, *Group Theory and Quantum Mechanics* (McGraw-Hill, New York, 1964).
- ⁴⁰ R. D. Duncan and C. A. R. Sá de Melo, Phys. Rev. B **62**, 9675 (2000).
- ⁴¹ J. H. Schon, C. Kloc, and B. Batlogg, Nature **406**, 702 (2000).
- ⁴² J. H. Schon, C. Kloc, and B. Batlogg, Nature **408**, 549 (2000).
- ⁴³ Y. Maeno, T. M. Rice, and M. Sigrist, Physics Today **54**, 42 (2001).
- ⁴⁴ L. J. Buchholtz and G. Zwicknagl, Phys. Rev. B **23**, 5788 (1981).
- ⁴⁵ C. R. Hu, Phys. Rev. Lett. **72**, 1526 (1994).
- ⁴⁶ K. Sengupta, I. Zutic, H. J. Kwon, V. M. Yakovenko, and S. D. Sarma, Phys. Rev. B **63**, 144531 (2000).
- ⁴⁷ A. J. Leggett, Rev. Mod. Phys. **47**, 331 (1975).
- ⁴⁸ G. M. Danner and P. M. Chaikin, Phys. Rev. Lett. **75**, 4690 (1996).
- ⁴⁹ In the calculation of $\chi_{mn}(T, H)$ the full effect of the presence of vortices need to be incorporated. A microscopic calculation of $\chi_{mn}(T, H)$ taking into account the spatial inhomogeneities introduced by the magnetic field and vortex core states is underway.
- ⁵⁰ Vortex core states are not as normal as the normal state of the superconductor, they have a lot of structure even in conventional singlet “s-wave” superconductors. Vortex core states in singlet “d-wave” superconductors have also a rich structure. So it is expected that vortex core states in triplet “p-wave” superconductors are even richer in structure due to the additional spin degrees of freedom present. The vortex core structure will be discussed in a later publication.
- ⁵¹ C. Caroli, P. G. de Gennes, and J. Matricon, Phys. Lett. **9**, 307 (1964).
- ⁵² J. Bardeen, R. Kummel, A. E. Jacobs, and L. Tewordt, Phys. Rev. **187**, 556 (1969).
- ⁵³ L. Kramer and W. Pesch, Z. Phys. **269**, 59 (1974).
- ⁵⁴ S. Ullah, A. T. Dorsey, and L. J. Buchholtz, Phys. Rev. B

- 42**, 9950 (1990).
- ⁵⁵ F. Gygi and M. Schlüter, Phys. Rev. B **43**, 7609 (1991).
- ⁵⁶ C. A. R. Sá de Melo, Phys. Rev. Lett. **73**, 1978 (1994).
- ⁵⁷ M. Ichioka, N. Hayashi, N. Enomoto, and K. Machida, Phys. Rev. B **53**, 15316 (1996).
- ⁵⁸ M. Franz and Z. B. Tesanovic, Phys. Rev. Lett. **80**, 4763 (1998).
- ⁵⁹ C. A. R. Sá de Melo, Phys. Rev. B **60**, 10423 (1999).
- ⁶⁰ The two fluids are not strictly independent, because vortex core states depend on properties (like the order parameter behavior) outside and at the boundaries of the core.
- ⁶¹ B. S. Shivaram, T. F. Rosenbaum, and D. G. Hinks, Phys. Rev. Lett. **57**, 1259 (1986).
- ⁶² C. H. Choi and J. A. Sauls, Phys. Rev. Lett. **66**, 484 (1991).
- ⁶³ K. Mortensen, Y. Tomkiewicz, and K. Bechgaard, Phys. Rev. B **25**, 3319 (1982).
- ⁶⁴ I. J. Lee and M. J. Naughton, *The Superconducting State in Magnetic Fields: Special Topics and New Trends* (World Scientific, Singapore, 1998), chap. 14, pp. 272–295, (Edited by C. A. R. Sá de Melo).